This dissertation has been
microfilmed exactly as received 68-13,264

GORADIA, Chandrakant P., 1939-
SURFACE STATES AND THE GOLD-n-SILICON
SURFACE BARRIER.

The University of Oklahoma, Ph.D., 1968
Physics, solid state

University Microfilms, Inc., Ann Arbor, Michigan

Downloaded from SHAREOK. Persistent Handle URL: https://hdl.handle.net/11244/2356

THE UNIVERSITY OF OKLAHOMA

GRADUATE COLLEGE

SURFACE STATES AND THE GOLD-n-SILICON SURFACE BARRIER

A DISSERTATION

SUBMITTED TO THE GRADUATE FACULTY

in partial fulfillment of the requirements for the

degree of

DOCTOR OF PHILOSOPHY

BY

CHANDRAKANT P. GORADIA

Norman, Oklahoma

1968

SURFACE STATES AND THE GOLD-n-SILICON SURFACE BARRIER

APPROVED BY

Jack Reynolds

C. R. Haden

Robert J. Nelson

Joel Cox

DISSERTATION COMMITTEE

ABSTRACT

The work reported in this dissertation was an attempt at obtaining a better understanding of the behavior of gold-n-silicon surface barrier diodes. Low reverse current, high breakdown voltage Au-n-Si surface barrier diodes were fabricated by using certain combinations of etch quenchants and surface treatments. The effects of these etch quenchants, surface treatments and different ambient conditions on the surface properties of silicon were studied by performing low frequency field effect measurements on filament samples of silicon. A new ambient cycle was evolved in order to obtain the conductance minimum in the field effect measurements. Differential capacitance measurements were made in order to correlate the rectification characteristics of the surface barrier diodes with their diffusion potentials. These measurements were not successful due to slow charge migration on the silicon surface. A model of slow charge migration and the results of its experimental confirmation are presented. The correlation of the rectification characteristics to the density of fast surface states

and to the thickness of the interfacial layer is discussed. The roles of oxygen and water vapor in the formation of the diode are explained. A simple physical model of the surface barrier diode is presented which explains many of the observed effects.

ACKNOWLEDGMENTS

My sincere thanks are due to Dr. Jack Reynolds for his constant guidance and encouragement. He also contributed much material help in designing and building the equipment used in this research. I would also like to thank Drs. William N. Carr and Kenneth L. Ashley of the Electronic Sciences Center of the SMU Institute of Technology for allowing the use of their diamond saw. Mr. Eugene Jeffries cut the filament samples for field effect measurements. His help is greatly appreciated. Thanks are also extended to Mrs. Martha S. Dybas for typing this thesis.

Finally, thanks are extended to the National Science Foundation for providing the most vital contribution to this research, namely, funds.

LIST OF TABLES

Table Number		Page
1	Scheme for Naming the Surface Barriers.....	79
2	Data on Alpha-Particle Probing Experiment for Confirmation of Capacitance Relaxation Model.....	95
3	Surface Potential and Density of Fast Surface States Obtained from Field Effect Measurements.....	115

LIST OF ILLUSTRATIONS

Figure Number		Page
1	Pulse Height Spectrum for a Monoenergetic Beam.....	15
2	Metal-Semiconductor Contact in the Absence of Surface States.....	30-31
3	Energy Band Diagrams for the Space Charge in n-type Silicon.....	37
4	Surface Conductance of a Semiconductor Filament.....	45
5	Theoretical ΔG-Σ_{sc} Curve.....	49
6	Effect of Acceptor-like Surface States on the Energy Bands of n-type Silicon.....	53
7	Transient Behavior of Surface States.....	59
8	Metal-Semiconductor Contact in the Presence of Surface States.....	69-70
9	Mounting Arrangement of the Au-n-Si Surface Barrier.....	79
10	Curve Tracer Characteristics of Surface Barriers After One Week of Storage in Filtered Room Air.....	81
11	Curve Tracer Characteristics of Surface Barriers After Seven Months of Storage in Filtered Room Air.....	82
12	Reverse Characteristics of the NO Group of Surface Barriers.....	84

LIST OF ILLUSTRATIONS--Continued

Figure		Page
13	Reverse Characteristics of the AR Group of Surface Barriers	85
14	Reverse Characteristics of the BW Group of Surface Barriers	86
15	Time Relaxation of Capacitance for the Surface Barrier NON	91
16	Figure Illustrating the Capacitance Relaxation Model	92
17	Schematic Diagram of the Arrangement for the Field Effect Measurements	97
18	Representative Oscilloscope FE Curves for the BW and DI Groups of Surface Treatments	99
19	Experimental ΔG vs. Σ_{in} Curve for the NO Surface Treatment	113
20	Experimental ΔG vs. Σ_{in} Curve for the AR Surface Treatment	114
21	Figure Illustrating the Simultaneous Use of a Silicon Filament as a Surface Barrier and a Field Effect Sample	130

TABLE OF CONTENTS

Page

ABSTRACT..... iii

ACKNOWLEDGMENT..... v

LIST OF TABLES..... vi

LIST OF ILLUSTRATIONS..... vii

Chapter

I. INTRODUCTION..... 1

Operation as a Nuclear Counter..... 2
Useful Quality Criteria for Nuclear Spectrometry Applications..... 3
Need for Research on Au-n-Si Surface Barriers..... 5
Surface States..... 7
Unresolved Problems..... 8
Motivation for the Present Research..... 13

II. THE GOLD-n-SILICON SURFACE BARRIER AS A NUCLEAR RADIATION COUNTER..... 14

Depletion Width..... 14
Resolution..... 15
Noise in Junction Counters..... 16

Statistical Fluctuations in Ionization..... 16
Incomplete Charge Collection..... 18
Thermal Noise..... 19
Noise Due to Reverse Current..... 21

Optimization of Total Noise..... 24
Breakdown Voltage..... 25
Summary..... 26

III. THEORY..... 29

Schottky Theory of a Metal-Semiconductor Contact in the Absence of Surface States..... 29
Theory of the Semiconductor Space Charge Region..... 36
Excess Surface Carrier Densities..... 42
Surface Conductance of the Space Charge Region..... 44
Theoretical ΔG versus Σ_{sc} Curve..... 48
Surface States..... 52
Theory of the Low Frequency AC Field Effect..... 63
The Au-n-Si Surface Barrier in the Presence of Surface States..... 67

IV. EXPERIMENTAL WORK ON Au-n-Si SURFACE BARRIERS..... 75

Fabrication..... 75

Pre-etch Preparation..... 76
Etching and Quenching..... 77
Surface Treatments..... 77
Gold Evaporation and Contacts..... 78

Identification Scheme..... 80
Reverse Current-Voltage Characteristics..... 80
Differential Capacitance Measurements for the Evaluation of the Diffusion Potential..... 88
Investigation of Capacitance Relaxation Effect by Alpha Particle Probing Experiment.... 90

V. FIELD EFFECT MEASUREMENTS..... 96

Introduction..... 96
Experimental Arrangement..... 96
Preparation of the Silicon Samples..... 102
Field Effect Measurements..... 106
The Ambient Cycle..... 109
Results of the Field Effect Measurements..... 111

VI. DISCUSSION..... 116

Inference from the Current Voltage Characteristics and Field Effect Measurements..... 116
Model for the Au-n-Si Surface Barrier in the Presence of Surface States..... 121
Conclusions..... 127
Recommendations for Further Research..... 129

REFERENCES..... 131

SURFACE STATES AND THE GOLD-n-SILICON BARRIER

CHAPTER I

INTRODUCTION

The gold-n-silicon surface barrier is a specific example of a general metal-semiconductor contact. It has been widely used during the last decade in the field of nuclear spectrometry. Although it was the first type of semiconductor junction counter to be used in nuclear spectrometry[1], its behavior and principle of operation are the least understood among all types of semiconductor junction counter.[6] However, the surface barrier counter offers an important attraction in that it is basically very simple to fabricate, requiring very little sophisticated equipment. Therefore, it can be easily fabricated in any well-equipped laboratory. Besides, the surface barrier counter offers some advantages over other types of nuclear counter in certain applications.[5]

Basically, an Au-n-Si surface barrier consists of a thin (100-500Å) gold film vacuum-evaporated on one surface of an etched disc of n-type silicon to which a non-rectifying contact is made at the other surface. A potential barrier is formed at the gold-n-silicon interface which exhibits electrical rectification characteristics. Electrically, such an Au-n-Si surface barrier

behaves very much like a one-sided step p-n junction, with the gold electrode behaving like the heavily doped p-side of the junction. The space-charge region which is depleted of free charge carriers, also known simply as the depletion region, lies exclusively within the n-type silicon and extends inwards from the Au-Si interface. The voltage drop due to the potential barrier takes place over the surface space-charge region. Hence the name surface-barrier.

Operation as a Nuclear Counter

When a reverse voltage bias is applied to the surface barrier (gold electrode at a negative potential with respect to the silicon), then the width of the depletion region increases as the square root of the reverse voltage. For a good surface barrier, the magnitude of the reverse current density will be extremely small, typically less than 1 $\mu A/cm^2$ for several hundred volts reverse bias. Thus, almost the entire reverse voltage drops across the depletion region, making it a high electric field region. If an ionizing particle such as an alpha particle is now incident through the gold film and is completely stopped within the high field region, then all the hole-electron pairs created by the ionizing particle will be swept away by the high electric field and a net charge will be collected at each electrode.

If the ionization density along the track of the incident particle is not exceedingly high as with the case of heavy ions or fission fragments, then McKay[2] has shown that there is no columnar recombination or capture of the free carriers within the depletion

region so that all the hole-electron pairs created will be collected.

If E is the energy of the incident particle and ε is the average energy required to create a hole-electron pair, then the number of free carrier pairs created will be E/ε. With suitable electronics such as a charge-sensitive amplifier, the collected free carrier charge will give rise to a voltage pulse which is proportional to the incident charged particle energy. A multi-channel pulse height analyzer can then sort out the voltage pulses into appropriate energy intervals giving rise to an energy spectrum.

This, in essence, is how an Au-n-Si surface barrier is used in nuclear spectrometry. In this application, it is used as a detecting device and behaves much like an ionization chamber whose basic function is to collect charge proportional to the incident particle energy. In conformity with common usage, the surface barrier, in its application in nuclear spectrometry, will be referred to simply as a detector or counter although a more appropriate name would be a solid state ionization chamber.

Useful Quality Criteria for Nuclear Spectrometry Applications

The most important criteria for determining the quality of a surface barrier in relation to nuclear spectrometric applications are listed below. These are discussed in detail in Chapter 2.

1. Resolution. The resolution of a nuclear counter is a measure of its ability to distinguish between two closely separated energies of the incident particle. The resolution is usually

measurable only for the system as a whole, that is, including the electronics. However, quite often, it is the detector which contributes the most to the loss of resolution. The loss of resolution is caused mainly by random electrical noise present in the detector although there will be a certain lower limit of noise present inherently due to the statistical nature of hole-electron creation by the ionized particle. As will be shown in Chapter 2, a good measure of the detector noise is its amount of reverse current at the voltage bias under consideration. In general, the larger the reverse current, the more the noise and the poorer the resolution.

2. Depletion Width. For energy spectrum measurements of nuclear radiations, it is obviously necessary that the incident ionizing particle lose all its energy within the high field region. This means that for radiations such as beta rays of energy $\geq$ 1MeV and high energy protons etc., the depletion width must be of the order of several millimeters. A large depletion width also helps in reducing the thermal noise by reducing the detector capacitance. For a fixed resistivity of the silicon material, the depletion width is proportional to the square root of the reverse voltage. The maximum useful depletion width is then governed by the maximum value of the reverse voltage up to which the noise remains within the required limits. Usually, the reverse breakdown voltage is taken as a criterion for judging the maximum available depletion width.

3. Stability. It is often necessary, as in the case of alpha spectrometry, to operate the detector under a vacuum. During normal storage and operation, the detector will be exposed to varying amounts of oxygen and moisture in the atmospheric air, and to other gases and vapors. For long term utility, the operational characteristics of the detector should remain stable under different ambient conditions.

Need for Research on Au-n-Si Surface Barriers

Considerable success has been achieved in making surface barriers which have the properties listed above, namely, low reverse current, high breakdown voltage, relative immunity against ambient changes and insensitivity to storage time. For example, surface barriers have been reported[3,4] with reverse current densities of less than 1 $\mu A/cm^2$ at about 1500-2000 volts reverse bias at room temperature and much less current at lower temperatures. Also, breakdown voltages as high as 4000-5000 volts have been achieved and for very high resistivity material, a depletion width of 3.5 to 4 mm has been reported.[3] However, commercially available counters do not usually exceed 2 mm depletion width. Insensitivity to ambient changes has been possible by special encapsulation techniques using epoxy.[5]

In spite of all this success, it can be said that the fabrication techniques are based more on empirical observations than on scientific knowledge.[5,6,7] The yield of good surface barriers is very low and surface barriers such as those reported

above are rather rare and expensive. Most surface barriers are extremely sensitive to ambients, especially moisture and other chemical vapors, become very noisy or break down at very low voltages in a vacuum, and change characteristics with time. Good surface barriers require special surface treatments. Hence the need for fundamental research on the basic physical processes of surface barrier operation.

The research reported here is concerned more with the fundamental physical processes of operation of an Au-n-Si surface barrier than with its applications in nuclear spectrometry. It is true that the starting point for this research was the motivation to put the fabrication procedure of surface barrier counters on a more scientific basis, thereby improving the yield and reducing the cost, and to improve the state-of-the-art of surface barrier counters. However, the research was fundamental and could be more appropriately termed as research on the physics and chemistry of silicon surfaces, using the Au-n-Si contact as a tool.

Only a clear understanding of silicon surfaces and of metal-silicon contacts can lead to a scientific foundation for the fabrication, maintenance and operation of surface barrier counters. In order to obtain such a clear understanding, we must turn to some of the unresolved problems about the Au-n-Si surface barrier. These problems are also shared by many other metal-semiconductor contacts and they all arise due to what are known as surface states.[11-13]

Surface States

Surface states are localized electron energy levels within the forbidden band and are located at the semiconductor surface and within or at the outer surface of a layer of adsorbed atoms. Two types of surface states, fast and slow, are known to exist.[8] The fast states are generally associated with the termination of the crystal lattice and defects and impurities at the semiconductor surface, and the slow states with the adsorbed atoms. Both fast and slow states can be either donor-like or acceptor-like. A donor-like surface state is electrically neutral when filled and positive when empty. An acceptor-like surface state is electrically neutral when empty and negative when filled. Fast states have a relaxation time (time required to fill or unfill a surface state) of 10^{-5} sec. or less whereas for slow states, it ranges from several milliseconds to several hours. Three important quantities characterize a surface state, namely, its energy position in the forbidden band, its density, and its relaxation time. All of these quantities are sensitive functions of several different physical and chemical factors.

In the absence of surface states, the theory of the Au-n-Si surface barrier would be very simple. The diffusion potential and the current-voltage characteristic are then given by the Schottky theory[9,10] which is discussed in greater detail in Chapter 3. The rectification characteristics would be stable with respect to time and ambient conditions. However, it is found in

reality that surface states control the behavior of most metal-semiconductor contacts.[14,15] The presence of surface states has given rise to a wealth of observed phenomena and has created immense difficulties, both in theory and experiment, in the study of metal-semiconductor contacts.

Unresolved Problems

The following are the important unresolved problems pertaining to the Au-n-Si surface barrier.

1. The rectification characteristics of a surface barrier depend strongly on the ambient conditions. It has been found from experience that a freshly evaporated gold contact on freshly etched silicon will not be strongly rectifying until after sufficient exposure to air or oxygen.[17] If one starts measuring the reverse current-voltage characteristics soon after exposure to air, one finds the reverse current at a given voltage to reduce by two or three orders of magnitude over a period of days. This is the so called forming or aging period for surface barriers.

There is no general agreement regarding the sequence or amount of exposure. A sufficient exposure after etching but prior to gold evaporation is considered adequate by some[18] whereas others[15] maintain that only post-evaporation exposure is useful in the formation of a good rectifier. Another aspect of ambient-sensitivity is that even after proper aging, the reverse characteristics are very sensitive to the ambient. For example, the reverse current at a given voltage changes considerably upon

exposure to a high vacuum or to vapors of NH_3, HF, halogens etc. Also, a certain amount of moisture in the air has been found to be necessary during the aging period.[3] Perfectly dry air does not yield good rectifiers. This apparently is paradoxical since for n-type silicon, dry air is known to make the surface more p-type whereas moisture tends to make it more n-type. Evidently, both air and moisture are needed to yield good rectifiers.

The problem here is to gain a thorough understanding of the physical reasons behind these observations as well as to devise means by which surface barriers can be made ambient-insensitive. One method of achieving ambient-insensitivity, with limited success, has consisted of encapsulation of the surface barrier in an inert impermeable material such as epoxy.

2. Chemical surface treatments prior to gold-evaporation have also been found to influence the rectification characteristics[3,19] significantly. Certain chemical treatments have been experimentally found to yield better rectifiers with high reverse breakdown voltages than others. However, there is no general agreement among research workers regarding their comparative merits. No scientific explanation exists for the effects of surface treatments. Both the ambients and the surface treatments are intimately tied to the surface states. The problem then is to investigate the relation of the ambients and surface treatments to the energies and densities of fast and slow surface states and of the surface states to the rectification characteristics.

3. In spite of the presence of surface states, there is still some relation between the rectification characteristics and the work function of the metal used. Gold is generally used because it has been experimentally found to give good rectification characteristics, but Siffert and Coche[15] have shown that chromium and platinum can be used equally well. When a particular metal such as gold has been chosen, one need not be concerned about the metal work function anymore. However, it is necessary to understand the role played by gold in giving good rectification characteristics. For example, Siffert and Coche believe that the higher work function of gold compared to that of silicon causes an electric field between the gold and silicon which aids the fixation of negative oxygen ions to the silicon surface, thereby forming an inversion surface layer on the n-type silicon. This is why they believe that only post-gold-evaporation exposure to air is useful. They have also shown that after sufficient exposure to air (up to one year), almost any metal forms a strongly rectifying contact regardless of its work function. This suggests that the role played by the metal (including gold) is simply that of an electrode or ohmic contact to the p-type surface layer; the metal is not the cause of the surface barrier which is clearly there due to surface states. The problem here is to verify to what extent this last statement is true.

4. Having established the dependence of the rectification characteristics on the ambients, surface treatments and metal work

function, it is necessary to determine their relative importances. For example, Walter and Boshart[19] rate the relative importance of surface treatments, adsorbed gases and metal work function in that decreasing order. Further experimental evidence is necessary for such a ranking.

5. There have been conflicting reports regarding the relation between the reverse characteristics and the surface barrier heights. Walter and Boshart[19] found that the larger the barrier height, the lower the reverse saturation current. Gibbons[20] found no such correlation. Also, the relation between the barrier height and the reverse breakdown voltage is not known. Thus, more investigation is necessary in this matter.

6. Archer[21] has reported that when silicon is etched in an HNO_3-HF etchant, a stain film is formed on the surface whose thickness depends on whether the etching reaction is quenched by deionized water or by an excess of HNO_3 followed by rinsing in deionized water. He reported the film thickness to range from 10-20 Å for HNO_3 quenched reactions to about 100-200 Å for deionized water quenched reactions. The exact composition of the films was not determined but they were believed to be either elemental silicon or some form of silicon hydride for n-type silicon. It is necessary to investigate the relation of the film-thicknesses, that is, of different quenchants to the rectification characteristics. The almost universal acceptance of deionized water as the quenchant should therefore be questioned.

If Archer's results are correct, then one is faced with two interfacial layers between the gold and the silicon. One layer is due to chemisorbed atoms and another is due to the quenchants and/or post-etch surface treatments. Both of these interfacial layers could be the seats of surface states and could thereby control the rectification characteristics. Very little information is available on the composition, thickness and dielectric constant of, and the energy and density of surface states (fast and/or slow) in either interfacial layer. It is certain, however, that both the interfacial layers must be transparent to free charge carriers in order to account for the high forward currents.

Cowley and Sze[22] have proposed a theory which relates the surface barrier height to the work functions of the metal and semiconductor, to the density of surface states and to the thickness of the interfacial layer. Their theory assumes only one interfacial layer, without regard to its nature or origin, and makes no distinction between fast and slow surface states. Walter and Boshart[19] have attempted to extend this theory to the case of two interfacial layers and they consider both fast and slow states. The problem is, however, that most of the parameters used in either theory are of unknown magnitudes, so that one can only make educated guesses regarding their values.

Qualitatively, however, their theory predicts that the larger the density of fast states and/or the thickness of the inner interfacial layer, the smaller will be the dependence of the

semiconductor surface potential on the ambient and/or the metal work function. An experimental confirmation of this prediction is necessary.

Motivation for the Present Research

Having discussed the unresolved problems pertaining to the Au-n-Si surface barrier it is now appropriate to state the motivation behind the research reported in this thesis. Specifically, this motivation was threefold:

1. To make a comparative evaluation of the different techniques used for the fabrication of Au-n-Si surface barriers.

2. To shed light on some of the unresolved problems mentioned above, especially those pertaining to the effects of ambients, quenchants and surface treatments on the rectification characteristics, and to investigate the relation between the barrier height and the rectification characteristics.

3. To develop a model for the Au-n-Si surface barrier, incorporating surface states, which can explain the observed effects.

CHAPTER II

THE GOLD-n-SILICON SURFACE BARRIER AS A NUCLEAR RADIATION COUNTER

The principle of operation of an Au-n-Si surface barrier as a nuclear counter has been discussed in Chapter I. The criteria which determine the quality of a surface barrier were also listed there. These will now be discussed in greater detail.

Depletion Width

For a homogeneously doped n-type silicon surface barrier at room temperature the depletion width is given by the relation

$$d = 5.3 \times 10^{-5}(\rho_n V)^{1/2} \text{cm} , \qquad (1)$$

where ρ_n is the resistivity of the silicon in ohm-cm and V is the total reverse voltage, including the diffusion voltage.[5] It is therefore seen that in order to obtain a large depletion width, it is necessary to use a high resistivity material and a large reverse voltage. For a resistivity of 10,000 ohm-cm, a depletion width of 5 mm would require a reverse voltage of approximately 10,000 volts. Hence the necessity of a high breakdown voltage when a large depletion width is desired. It is also necessary that the reverse

current at such high voltages be low in order to minimize noise.

Resolution

The resolution of a nuclear counter indicates its quality and usefulness as a charged particle energy spectrometer. It is a measure of the minimum separation in energy that can be unambiguously resolved.

Consider a monoenergetic beam of charged particles incident on the counter. Then ideally, the output voltage pulses should all be of the same magnitude. In practice there will be some spread in the pulse heights and the pulse height spectrum will appear similar to that shown in Figure 1.

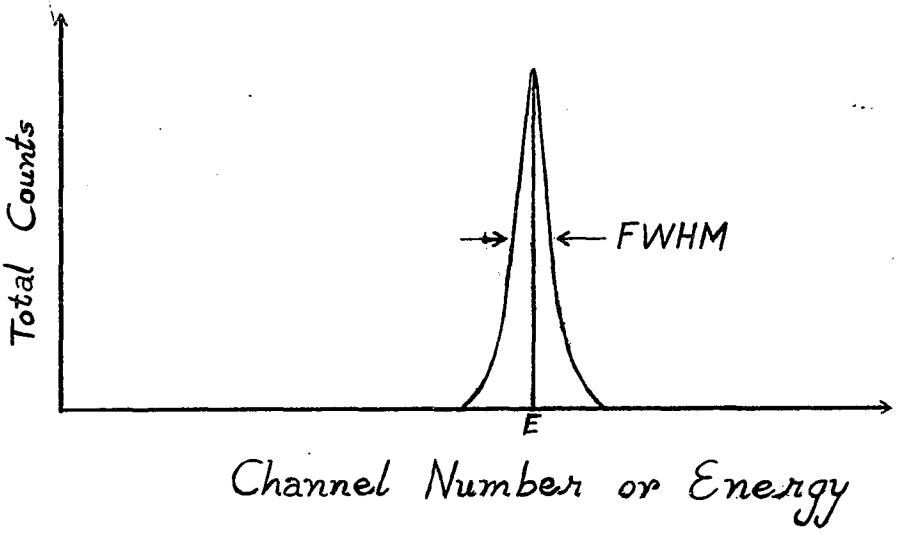

Figure 1

Pulse Height Spectrum for a Monoenergetic Beam

The resolution has been conventionally defined in two ways.

1. If the peak of the spectrum occurs at a certain energy, say E MeV, then the absolute width of the spectrum curve in MeV (or KeV) at half the value of the peak counts is called the full width at half maximum (FWHM) resolution.

2. When the full width at half maximum resolution defined above is expressed as a percentage fraction of the peak energy E , then this percentage fraction is called the fractional width at half maximum resolution and is also denoted as FWHM.

It will be realized that the above definitions of resolution denote the overall resolution of the composite nuclear spectrometer system including the electronics. Noise present in both the counter and the electronics (mainly in the charge-sensitive preamplifier) will contribute to a poor resolution. If the noise in the electronics is small compared to that in the counter, the resolution is then controlled almost entirely by the counter. This may often be the case in practice.

Noise in Junction Counters

There are several causes of noise in a rectifying junction counter. These are discussed in the following pages.

Statistical Fluctuations in Ionization

Since the creation of hole-electron pairs by an incident charged particle is a statistical process, a beam of monoenergetic particles will give rise to some spread in the pulse heights

obtained. If N hole-electron pairs are created by a charged particle as a result of N entirely independent ionizing events, then the standard deviation in N would be $N^{1/2}$. In reality, the events are not all independent and the standard deviation is given by

$$\sigma = (FN)^{1/2} , \tag{2}$$

where F is the Fano factor which is less than one.[5] Equation (2) serves as the definition of the Fano factor when σ is the actually observed standard deviation. The percentage standard deviation is then given by

$$\frac{\sigma}{N} = \left(\frac{F}{N}\right)^{1/2} , \tag{3}$$

and since $N = \frac{E}{\varepsilon}$, this becomes

$$\frac{\sigma}{N} = \left(\frac{F\varepsilon}{E}\right)^{1/2} . \tag{4}$$

If the pulse height spectrum is approximately gaussian, then the fractional width at half maximum resolution is 2.35 times that given by (4).

It is seen from (4) that the lower the energy required to create a hole-electron pair, the better the resolution.

In order to have an idea of the amount of noise contributed by statistical fluctuations, it can be calculated that for a 1 MeV charged particle beam incident on a silicon counter, and

for $F = 0.1$, the full width at half maximum resolution will be 0.4 KeV. In practice, the Fano factor for silicon is believed to lie between 0.13 and 0.06.[29] This value gives the theoretical limit of the best resolution possible with a given semiconductor material, due to inherent limitations.

Incomplete Charge Collection

Incomplete charge collection can occur in three different manners. First, if the ionization density along the particle track is very large, as with a fission fragment, columnar recombination can take place and those charge carriers lost along the particle track contribute a negligible amount to the signal pulse. Second, if the lifetime of some free charge carriers is not large enough for them to traverse the complete electric field region, then their contribution to the signal will only be a partial contribution. Such a case can arise in a large depletion width counter with insufficient carrier lifetime. Third, if the particle track is longer than the active region of the counter, then quite naturally there will be incomplete charge collection.

The loss of resolution due to columnar recombination is in most cases smaller than that due to statistical fluctuations in N. The second factor causes the same amount of loss of resolution as the statistical fluctuations in N and is important only when the active width of the counter is large compared to the carrier drift length. Regarding the third case, if the counter is to be

used for total energy spectrometry, then it is of no value to use one whose depletion width is less than the particle track length in the counter material. If, on the other hand, the counter is to be used for dE/dx measurements, then this problem does not arise since in a dE/dx counter, the depletion region covers the entire width of the counter.

Thermal Noise

Thermal noise, or Johnson noise, occurs in any conductor due to the thermal velocities of charge carriers, regardless of whether a current is flowing through it or not. The preamplifier connected to the counter will see this noise as an r.m.s. voltage whose value is given by

$$\overline{V}^2 = \frac{kT}{C} \quad , \tag{5}$$

where k is the Boltzmann constant, T the absolute temperature of the counter and C is the total capacitance of the counter including stray capacitance of the leads.[5] The amount of line broadening or loss of resolution is then defined as that energy ΔE of the incident particle which will create a voltage pulse of the same height as the r.m.s. thermal noise voltage. It is given by

$$\Delta E = \frac{\varepsilon}{q} (kTC)^{1/2} \quad . \tag{6}$$

For silicon at room temperature, this gives

$$\Delta E = 1.4\ C^{1/2}\ \text{KeV}\ , \tag{7}$$

where C is measured in pf.

It is seen from this equation that to keep the effect of thermal noise on the resolution to a minimum, the total capacitance of the counter must also be kept a minimum. If the stray capacitance in the leads is neglected, and if the counter is treated as a parallel plate capacitance of plate separation equal to the depletion depth d, then the junction capacitance per unit area of the counter is given by

$$\frac{C}{A} = \left(\frac{\varepsilon_r \varepsilon_o q N_D}{2V}\right)^{1/2} \tag{8}$$

or equivalently, by

$$\frac{C}{A} = \left(\frac{\varepsilon_r \varepsilon_o}{2\rho_n \mu_n V}\right)^{1/2}\ , \tag{9}$$

where, ρ_n is the resistivity of the n-type silicon, μ_n is the electron mobility, N_D the donor density, ε_r the dielectric constant of silicon, ε_o the permittivity of free space, and V is the total voltage.

It is seen that a large depletion width is useful in reducing the thermal noise due to a reduction in capacitance. It can be calculated that for a 1 cm^2 silicon junction at room temperature, the depletion width must be at least equal to 214 microns in order to keep the line boradening due to thermal noise

within 10 KeV.[5]

Noise Due to Reverse Current

It has not been possible, so far, to calculate the amount of line broadening or loss of energy resolution due to reverse current as was done with the other sources of noise. There are at least three different sources of reverse current and each can contribute to noise in a different manner, independent of the other two. There does not exist an exact proportionality between the amount of reverse current and the amount of noise since the total current noise depends on the relative proportions of the individual sources of reverse current. Thus, for example, 0.5 μA reverse current due to recombination in the depletion region may result in greater noise than 1 μA of surface leakage current.[23] It is quite true, however, that for a given device, or a given set of devices prepared in basically the same manner, the noise will in general be proportional to the reverse current. Thus, the amount of reverse current is a useful measure of the noise in a surface barrier counter. Let us now consider the three different sources of current noise in some detail.

I. Bulk Diffusion Current

The minority carriers present in the undepleted region will constantly diffuse into the depletion region and give rise to a room temperature bulk diffusion current density given by

$$I_d = 7\text{x}10^{-3}\rho_n L_p \tau_p^{-1} \ \mu A/cm^2 \ , \qquad (10)$$

where ρ_n is the n-type bulk resistivity in ohm-cm, L_p is the hole diffusion length in cms and τ_p is the hole lifetime in μsec. This equation is valid when the width of the undepleted region is large compared to L_p and when there is no surface recombination. Equation (10) clearly shows the need for a bulk material with a large minority carrier lifetime but it also shows that in order to reduce I_d, the bulk resistivity must not be too high. In practice, high bulk resistivities are chosen anyway to obtain large depletion widths at reasonable voltages. The bulk diffusion current can be minimized by totally depleting the counter provided that this does not cause a problem due to carrier injection from the base contact.

II. Reverse Current Due to Charge Generation in the Depletion Region.

This current arises from the thermal generation of charge carriers within the depletion region via generation and recombination centers. For this case, the theory of Sah, Noyce and Shockley[25] gives, at room temperature,

$$I_g = 6\text{x}10^{-2}(\rho_n V)^{1/2}\tau_p^{-1} \ \mu A/cm^2 \ , \qquad (11)$$

where V, ρ_n, τ_p have been defined earlier. It is seen that I_g is proportional to the depletion width. Here again, a large

minority carrier lifetime in the bulk material is of considerable advantage. Although both I_d and I_g increase with the resistivity, ρ_n, of the starting material, this increase may not be as large as it appears since in float-zone refined silicon the minority carrier lifetime τ_p also tends to increase with ρ_n.

III. Surface Leakage Current

This current is due to a conducting shunt path between the gold electrode and the base electrode due to the space charge region which exists under the entire surface of the counter. The cause of this space charge region and its theory are discussed in Chapter 3. The width and conductance of this space charge region depend on the amount of bending of the energy bands at the surface, that is, on the surface potential. If an inversion layer exists at the surface due to surface treatments or ambients, then the shunt path will have a relatively large conductance.

It is possible to minimize this surface current by causing the surface potential at the free surface of the silicon to be lower in magnitude than the diffusion potential under the gold electrode. One way of doing this is by encapsulating the counter in an epoxy resin with an amine type hardener which prevents the formation of an inversion layer under it. A p-n junction will then be formed between the inverted space charge region below the gold electrode and the non-inverted space charge under the free surface.[5] Another method of minimizing the surface leakage current is by using certain surface treatments, as was done in the work reported here.

It is seen that the total reverse current depends on several factors. Under certain conditions, one or more of the sources of the reverse current can be eliminated or minimized. For example, Langmann and Meyer[26] have shown that with proper encapsulation, the reverse current is almost totally made up of diffusion and generation currents. Minimum surface leakage current has also been achieved by using surface treatments instead of encapsulation.

Optimization of Total Noise

Having considered the different sources of noise in some detail, we can now draw the following general conclusions:

1. Most sources of noise increase with the active area of the counter.

2. It is extremely important to have a starting material with as large a minority carrier lifetime as possible. It is in this regard that surface barriers are superior to the diffused junction counters. When counters are desired with large areas and large depletion widths, both these factors give rise to increased current noise. The only other controllable variable is the minority carrier lifetime. Now, starting with high minority carrier lifetime silicon, it is possible to maintain it in a surface barrier but not in a diffused junction counter. The fabrication of a surface barrier is performed at room temperature whereas the high temperature required for the diffusion process in a diffused junction counter degrades the minority carrier lifetime.

3. In order to obtain a large depletion width, it is better to use high resistivity material than to use an extremely high voltage. This is because of the fact that a higher resistivity may be accompanied by a better minority carrier lifetime and also because a high voltage may give rise to microplasma breakdown noise due to surface inhomogeneities.

4. There are essentially two conflicting factors in the optimization of counter noise. The thermal noise reduces with an increase in depletion width due to reduction in capacitance. However, the current noise increases with depletion width. Thus, in order to optimize the overall counter noise, one must use that reverse voltage which will give the least overall noise for a given counter. When an application demands a large depletion width, the current noise will dominate over the thermal noise. One must then try to minimize the current noise by fabricating the counter out of high resistivity high lifetime material and using the proper surface treatments and/or encapsulation techniques. However, in the case of an application like alpha particle spectrometry where a large depletion width is not required, it is in general possible to minimize the overall noise.

Breakdown Voltage

As discussed earlier, large depletion width counters require large reverse bias voltages. At large electric fields in the depletion region, avalanche breakdown will occur. It should be

noted, however, that in general there will be two depletion regions in the surface barrier counter, namely, (1) the main surface barrier depletion region under the gold electrode and (2) the depletion region at the junction between the free surface and surface barrier space charges. The free surface is that part of the surface which is exposed to the ambient. When this second depletion region breaks down, a space charge limited surface current will then flow and its magnitude will be controlled by the conductance of the free surface space charge. Depending on the conditions at the free surface, it is often possible for the space charge junction to break down at a much lower voltage than the surface barrier. This is the reason why the breakdown voltage is so ambient sensitive. In many cases, there may also be inhomogeneities in the silicon surface or bulk where a breakdown may occur. Such inhomogeneities can produce large noise pulses without contributing much to the total average reverse current. Surface barriers with high breakdown voltages can be obtained by using certain chemical surface treatments and/or encapsulation.

Summary

In the light of the discussion presented in this chapter it is now possible to meaningfully define the three most important attributes of a good quality surface barrier counter. First, and most important, is the resolution of a counter. It is true that

all possible applications do not demand the same amount of high resolution; neither is it always possible to achieve it, since the resolution depends on the active area, depletion width, the temperature of operation, and the degree of sophistication of the electronics.

No mention was made earlier of the temperature of operation but it is true that the thermal noise as well as the sources of current noise can be considerably reduced by maintaining the counter at temperatures between the solid CO_2 and liquid nitrogen temperatures. However, it is a great disadvantage in terms of convenience and cost to have to operate at low temperatures. Besides, there is also the associated problem of preventing moisture condensation on the counter and the radioactive sample when the sample needs to be changed. It is for this reason that all effort was put into developing high-resolution counters which are operable at room temperature.

The second criterion for judging the quality of a counter is the maximum available depletion width. For a given resistivity of the starting material, this is governed by the maximum value of the reverse voltage to which the noise remains within the required limits. Here again, the application will determine the size of the depletion width which is necessary but a counter capable of having a large depletion width will be useful for more applications than one which is not.

Finally, the counter must be stable with respect to its

resolution and breakdown voltage over a long period of time as well as under vacuum. A vacuum is necessary for alpha and low energy beta spectrometry. Most surface barrier counters tend to become exceedingly noisy under a vacuum and also tend to break down at very low voltages.

The following general statements can be made regarding the fulfillment of the above three criteria in order to produce a good surface barrier counter.

1. High resolution at room temperature can be achieved with certain surface treatments when the starting material has a large minority carrier lifetime.

2. The same surface treatments which satisfy 1. also give rise to high breakdown voltages so that large depletion widths can be achieved when high resistivity starting material is used.

3. Proper encapsulation with epoxy resin after the right kind of surface treatment can prevent deterioration with time and under a vacuum environment.

CHAPTER III

THEORY

The theory of the Au-n-Si surface barrier will be presented in this chapter. First, the Schottky theory of a metal-semiconductor contact in the absence of surface states will be discussed in brief. Next, a theory of the semiconductor space charge region will be developed in regard to both surface channel conduction and the a.c. field effect. Finally, the gold-n-silicon surface barrier in the presence of surface states will be considered.

Schottky Theory of a Metal-Semiconductor Contact in the Absence of Surface States

The Schottky theory will not be presented in detail since it does not correspond to the real situation. However, it is still important because it shows how a metal-semiconductor contact can be expected to exhibit rectification characteristics.

Consider the specific case of a gold-n-silicon contact of the type shown in Fig. 2a. Figures 2b, c, and d show the energy band diagrams for this contact under thermal equilibrium (no current flow), forward voltage bias and reverse voltage bias respectively. Forward bias corresponds to the gold being at a positive potential

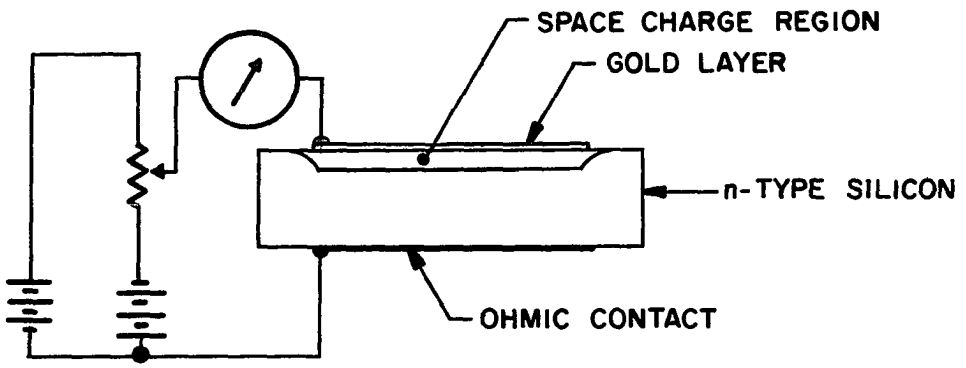

Fig. 2a Gold-n-Silicon Contact with Biasing Electrical Circuit

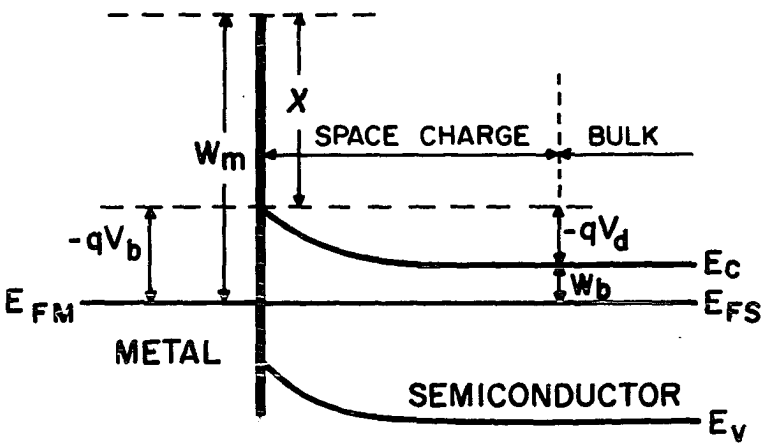

Fig. 2b Energy Band Diagram of the Au-n-Si Contact Under Thermal Equilibrium

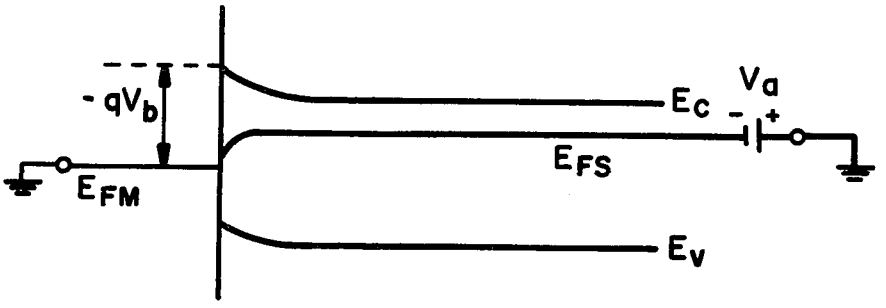

Fig. 2c

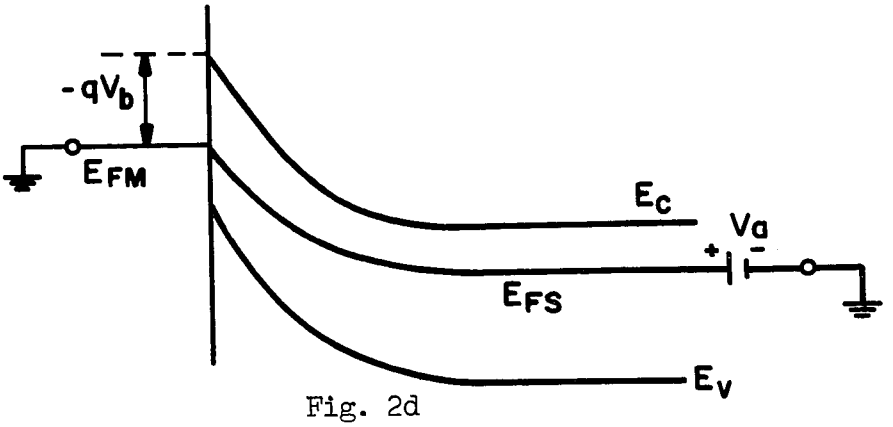

Fig. 2d

Fig. 2 (Cont'd) Energy Band Diagrams of a Forward Biased Au-n-Si Contact (c), and of a Reverse Biased Au-n-Si Contact (d).

Fig. 2
Au-n-Si Contact in the Absence of Surface States

with respect to the silicon and reverse bias corresponds to the opposite polarity conditions. It is important to note that these energy diagrams shown in Fig. 2 refer only to that region of the silicon which is directly under the gold-silicon interface. At the surface of silicon which is far removed from the gold, the energy bands will continue to be straight right up to the silicon surface since no surface states are assumed to be present.

First consider the case of thermal equilibrium as shown in Fig. 2b. Here, the higher work function of gold causes electrons to flow from the silicon to it until the two Fermi levels coincide, as demanded by the condition of thermal equilibrium. When this happens, an electrostatic field is set up between the negative surface charge on the gold and an equal amount of positive space charge in the silicon. The magnitude of the electric field must be such as to prevent further flow of electrons from the silicon to gold under equilibrium. The space charge extends to a non-negligible depth below the Au-Si interface due to the small number of free electrons in the silicon. The energy bands of the n-type silicon must be bend upwards in order to account for the variation of the free-electron density in the space charge region as a function of the distance from the surface. The amount of bending of the bands at the silicon surface is given by the diffusion potential V_d, as obtained from the equation:[10]

$$-qV_d = W_m - W_s = W_m - \chi - W_b \ , \qquad (12)$$

where q is the magnitude of the electronic charge, W_m, W_s are the metal and semiconductor work functions, χ is the electron affinity of the silicon and W_b is the energy difference between the bottom edge of the conduction band and the Fermi level in the silicon bulk (far removed from the surface). The very large micro-potential barrier due to χ and W_m is very small in width and is transparent to electrons due to quantum mechanical tunelling. V_d, which is the surface potential of silicon under the gold electrode under zero applied bias, is called the diffusion potential because under thermal euqilibrium, its magnitude is just sufficient to cause a drift current which exactly counteracts the diffusion current.

Although V_d is the true potential barrier against the flow of electrons from the silicon to the gold, it is customary to define the barrier height, V_b, as the energy required to take an electron from the Fermi level in the metal to the conduction band edge at the silicon surface. V_b is given by the equation:

$$-qV_b = W_m - \chi = -qV_s + W_b \quad . \tag{13}$$

We see from (12) that the Schottky theory predicts a surface potential barrier which depends on the difference between the metal and semiconductor work functions. Bardeen[11] was the first to propose an explanation of the observed lack of dependence of the diffusion potential on the metal and semiconductor work functions on the basis of surface states.

When a forward bias such as that shown in Fig. 2c is applied, the barrier height V_b remains constant but the silicon surface potential V_s decreases in magnitude so that an electron diffusion current flows from the silicon to the gold. The resistance to current flow is relatively small in this direction. However, when a reverse bias is applied, V_s increases in magnitude and the resistance to current flow is relatively very high in this direction. If the applied reverse voltage is large, then a high electric field will exist across the space charge region and it will sweep away any free carriers that are generated within or happen to diffuse into the space charge region. Hence a finite but small reverse current will flow.

Quantitatively, the Schottky theory gives the current-voltage characteristic to be:[9]

$$J_n = \sigma_n\left[\frac{2qN_D}{\varepsilon_r\varepsilon_o}(|V_d|+V_a)\right]^{1/2} e^{\frac{-q|V_d|}{kT}} x \frac{e^{\frac{-qV_a}{kT}}-1}{1-e^{\left[\frac{-2q(|V_d|+V_a)}{kT}\right]}}, \qquad (14)$$

where J_n is the current density, σ_n the conductivity of the n-type silicon, N_D the donor density, ε_r the dielectric constant of silicon, ε_o the permittivity of free space, V_a the applied voltage bias, positive when reverse and negative when forward, and the other quantities have been previously defined. This equation is valid only for a metal-semiconductor contact in which V_d is negative, that is, the metal work function is larger than that of

the n-type silicon. It is also assumed that minority carrier injection is negligible so that the current is due to a flow of electrons only.

The reverse current density given by the above equation is actually higher than the experimentally observed reverse current density by two or three orders of magnitude. It has been shown by Langmann and Mayer[26] that at room temperature, and in the absence of surface channel conduction, the reverse current can be quite accurately expressed as the sum of two components, viz., the bulk diffusion current given by (10) and the current due to charge generation in the depletion region as given by (11). The actual current-voltage characteristic thus differs from that predicted by the Schottky theory in two ways. First, the reverse saturation current is much smaller and secondly, its dependence on the diffusion potential V_d is much milder than the inverse exponential dependence given by (14). A recent improvement on the Schottky theory[9] can account for the smaller reverse saturation current but its relative lack of dependence on V_d can only be explained by the presence of surface states. It is evident that surface states make the Au-n-Si surface barrier behave more like a p-n junction diode than like a metal-semiconductor contact. Also, surface states make such a surface barrier sensitive to chemical treatments and ambients and create an additional source of reverse current through the surface space charge layer.

Theory of the Semiconductor Space Charge Region

A space charge will arise under the surface of a semiconductor whenever there is an electric field present at its surface. Such an electric field can arise in three ways: 1) by simply placing the semiconductor in a region of space containing an electric field due to some external source; 2) when the semiconductor is in the close proximity of a metal with a different work function than its own; and 3) when there is a surface sheet of charge due to electrons or holes bound in surface states.

Once a space charge is created, it has certain unique properties which do not depend on the manner in which it was brought about. Hence, in the following discussion, the properties of the space charge will be considered without regard to the specific agency causing it.

Consider the energy band diagrams of an n-type semiconductor as shown in Figures 3a and b. Fig. 3a corresponds to a positive space charge and Fig. 3b corresponds to a negative space charge. All the important parameters are shown in the figure.

The reference of energy is taken as the Fermi level E_F. The intrinsic Fermi level, which is given by

$$E_i = \frac{E_c + E_v}{2} + \frac{kT}{2} \ln\left(\frac{N_v}{N_c}\right) , \qquad (15)$$

is assumed to coincide with the electrostatic macropotential. A semi-infinite homogeneous crystal under thermal equilibrium is

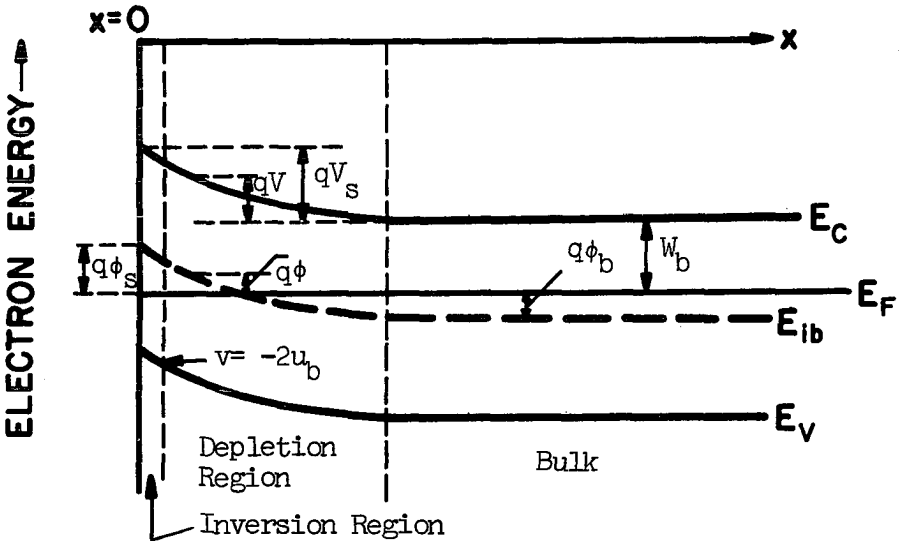

Fig. 3a Electron Energy Versus Distance from the Surface for a Semiconductor with positive Space Charge

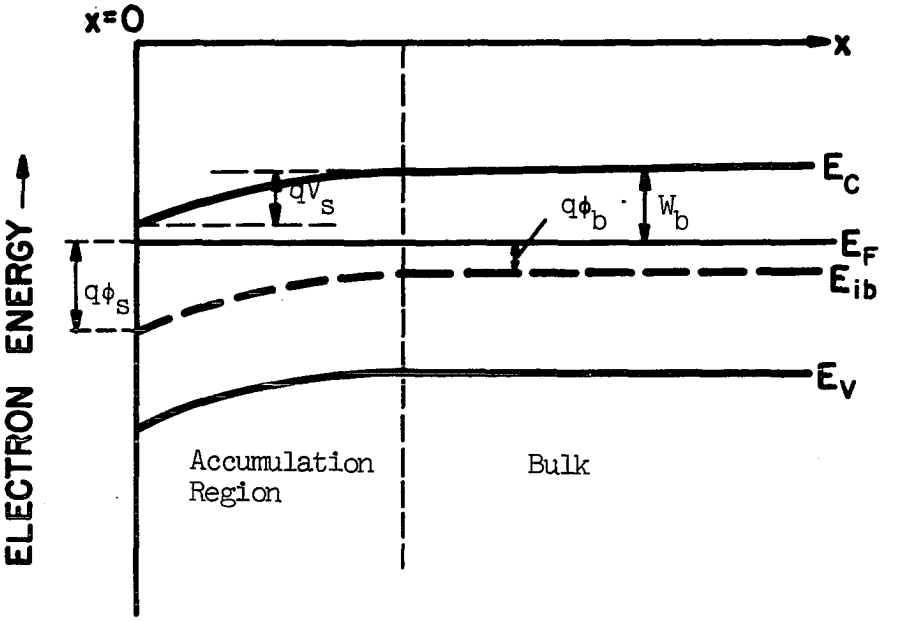

Fig. 3b Electron Energy Versus Distance from the Surface for a Semiconductor with Negative Space Charge

Fig. 3
Energy Band Diagrams for the Space Charge in n-type Silicon

assumed. The surface is represented by the plane $x = 0$ and the bulk by positive values of x. The electrostatic potential barrier as a function of x is then given by

$$V(x) = \frac{E_{ib} - E_i(x)}{q} \quad , \tag{16}$$

where E_{ib} is the value of E_i in the bulk, far removed from the surface. Thus, V will be negative when the bands bend up (positive space charge) and positive when the bands bend down (negative space charge). This is because of the negative charge on the electron; when its potential energy is positive its electrostatic potential is negative and vice versa.

The electrostatic potential with respect to the Fermi level is given by

$$\phi(x) = \frac{E_F - E_i(x)}{q} \quad . \tag{17}$$

It is more convenient to define dimensionless quantities v, u by the equations

$$v(x) = \frac{qV(x)}{kT} \quad ; \quad u(x) = \frac{q\phi(x)}{kT} \quad . \tag{18}$$

The carrier densities under thermal equilibrium can then be expressed as

$$n(x) = n_i e^{u(x)} = n_b e^{v(x)} \tag{19}$$

$$p(x) = n_i e^{-u(x)} = p_b e^{-v(x)} \quad , \tag{20}$$

where $n_b = n_i e^{u_b}$ and $p_b = n_i e^{-u_b}$ are the electron and hole densities in the bulk. It also follows from the definitions that

$$v(x) = u(x) - u_b \ . \tag{21}$$

The conditions $u(x) \gtrless 0$ correspond to $n(x) \gtrless p(x)$. When $u(x) = 0$, then $n(x) = p(x) = n_i$, the intrinsic carrier density. Also, $v(x) \gtrless 0$ corresponds to the energy bands bending down, no bending, and bending up respectively. At the surface, $x = 0$, the values of v , u , V and ϕ are denoted with a subscript s as v_s , u_s , V_s and ϕ_s respectively. Then for a homogeneously doped crystal, $v_s = 0$ means that the bands are straight right up to the surface. This is known as the flat-band condition.

When v_s and u_b are of the same sign, then the majority carrier density in the space charge region will be greater than that in the bulk and we get what is called an accumulation layer. When v_s and u_b are of opposite sign, we get either a depletion or an inversion layer. The space charge region up to the point where the minority carrier density is equal to the majority carrier bulk density (where $v(x) = -2u_b$) is called the depletion region. Between this point and the surface, the minority carrier density exceeds the majority carrier bulk density and this region is called the inversion layer. It is possible for the depletion region to extend right up to the surface if $|v_s| \leq |2u_b|$.

The condition of space charge neutrality in the bulk region gives

$$p_b + n_D = n_b + n_A \quad , \tag{22}$$

where n_A and n_D are the densities of ionized acceptor and donor atoms respectively. In the space charge region, the net space charge density will then be

$$\begin{aligned} \rho(x) &= q(p+n_D) - q(n+n_A) \\ &= q(p-p_b) - q(n-n_b) \quad . \end{aligned} \tag{23}$$

The variation of potential with the distance x from the surface is obtained by solving Poisson's equation which, in terms of the reduced potential v , can be given by

$$\begin{aligned} \frac{d^2v}{dx^2} &= - \frac{q\rho(x)}{\varepsilon_r \varepsilon_o kT} \\ &= \frac{-q^2}{\varepsilon_r \varepsilon_o kT} (p-p_b - n + n_b) \quad . \end{aligned} \tag{24}$$

This equation can be written as

$$\frac{d^2v}{dx^2} = \frac{1}{L^2} \left[\frac{\sinh(u_b + v)}{\cosh u_b} - \tanh u_b \right] , \tag{25}$$

where L is the effective Debye length which is defined as

$$L = \left[\frac{\varepsilon_r \varepsilon_o kT}{q^2 (n_b + p_b)} \right]^{1/2} \quad . \tag{26}$$

Multiplying both sides of (25) by $\frac{2dv}{dx}$ and integrating from $x = \infty$ in the bulk to $x = x$, we have, using the condition that $\frac{dv}{dx} = 0$ at $x = \infty$,

$$\frac{dv}{dx} = \frac{\pm F(u_b, v)}{L} \quad , \tag{27}$$

and integrating once more from $x = 0$, $v = v_s$ to $x = x$, $v = v(x)$, we get

$$\frac{x}{L} = \int_{v_s}^{v} \frac{dv}{\pm F(u_b, v)} \quad , \tag{28}$$

where

$$F(u_b, v) = \sqrt{2}\left[\frac{\cosh(u_b + v)}{\cosh u_b} - v \tanh u_b - 1\right]^{1/2} \quad . \tag{29}$$

The minus sign in front of $F(u_b, v)$ in (27) and (28) refers to $v > 0$ (bands bending down or negative space charge) and the plus sign is for $v < 0$ (bands bending up or positive space charge). The integration in (28) cannot be performed in a closed form except when $u_b = 0$ (intrinsic material). It must therefore be evaluated numerically.

The surface space charge density Σ_{sc} is defined as the total net charge in the space charge region per unit surface area. Σ_{sc} satisfies Gauss' law since the electric displacement vector $\overline{D}$ must vanish in the bulk.

Hence

$$\Sigma_{sc} = \varepsilon_r \varepsilon_o \left.\frac{dV}{dx}\right|_{x=0}$$

$$= \pm q(n_b + p_b) LF(u_b, v_s) \quad , \tag{30}$$

where $F(u_b, v_s)$ is the value of F evaluated at $v = v_s$. From (30), we see that the surface space charge density for silicon is strictly a function of the surface potential (V_s or v_s), the bulk carrier concentrations and the temperature and is independent of the nature or cause of the band bending agency.

Excess Surface Carrier Densities

By definition, the space charge density Σ_{sc} must also be given by

$$\Sigma_{sc} = \int_0^\infty q(p - p_b - n + n_b)dx \quad , \tag{31}$$

which can be written as

$$\Sigma_{sc} = q(\Delta P - \Delta N) \quad , \tag{32}$$

where

$$\Delta P = \int_0^\infty (p - p_b)dx \tag{33}$$

$$\Delta N = \int_0^\infty (n - n_b)dx \quad . \tag{34}$$

ΔP and ΔN are known as the excess surface carrier densities[27] which are defined as the number of mobile holes or electrons per unit area of the surface in excess of their number per unit surface

area under flat-band conditions. ΔP and ΔN will be of opposite signs. For example, for $v_s < 0$, (positive space charge), ΔP will be positive since the hole density in the space charge region is larger than in the bulk. However, the electrons will be depleted from the space charge region and ΔN will be negative.

As will be shown later, it is necessary to evaluate ΔP and ΔN individually in order to calculate the surface conductance of the space charge region. For this reason, (33) and (34) must be put into another form.

If we change the variable of integration in these equations from x to v, then we can put these in the form

$$\Delta P = p_b L \int_{v_s}^{0} \frac{e^{-v} - 1}{\pm F(u_b, v)} \, dv \tag{35}$$

$$\Delta N = n_b L \int_{v_s}^{0} \frac{e^{v} - 1}{\pm F(u_b, v)} \, dv \, . \tag{36}$$

In this form, ΔP and ΔN can be numerically evaluated on a digital computer for a range of values of the surface potential v_s, once the value of u_b is known. u_b is found from the type and resistivity of the semiconductor material by using the equation

$$u_b = \ln \frac{1}{q n_i \mu_n \rho_b} \, , \tag{37}$$

where ρ_b is the bulk resistivity, μ_n is the electron mobility for n-type material and n_i is the intrinsic carrier concentration

at the given temperature. Knowing u_b and n_b, p_b and L can be evaluated by using (19), (20) and (26).

It is seen that for a given u_b, ΔP and ΔN are single valued functions of the surface potential v_s and theoretical curves can be plotted of ΔP and ΔN over a wide range of both positive and negative values of v_s. Using (32), the surface space charge density Σ_{sc} can also be plotted as a function of v_s.

Surface Conductance of the Space Charge Region

The surface conductance of the space charge region, ΔG, at any surface potential v_s is defined as the change which occurs in the conductance, parallel to the surface, per square surface area of the semiconductor sample when the surface potential is changed from 0 to v_s. Effectively, ΔG is the conductance, parallel to the surface, per square surface area due to the excess surface carrier densities only, since it is the difference between the conductance per square surface area, parallel to the surface, when there is a space charge and the same quantity when the bulk carrier densities extend right up to the surface (flatband conditions).

Consider a semiconductor filament as shown in Figure 4, for which ℓ, w and d denote, respectively, its length, width and depth. The x, y, z axes are taken along d, w and ℓ respectively. Flatband conditions are assumed to prevail at all faces except the face $x = 0$ where we have a surface potential v_s. Let σ_s, d_s and σ_b, d_b denote, respectively, the average

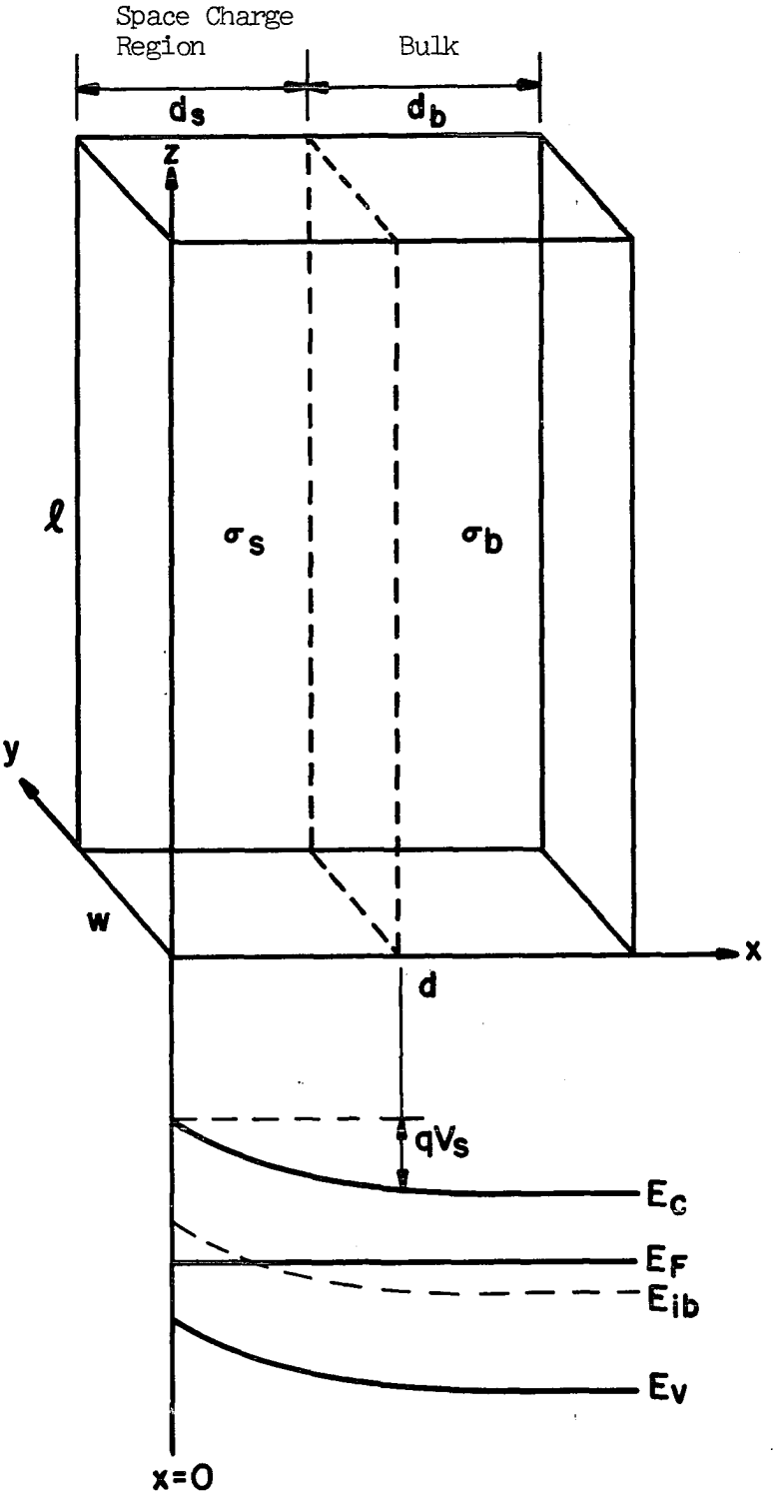

Fig. 4 Semiconductor Filament with Space Charge Region Under One Face. Explanation of Surface Conductance.

conductivities and depths of the space charge and bulk regions.

The conductance of such a filament along its length is given by

$$g = \frac{(\sigma_s d_s + \sigma_b d_b)w}{\ell} \quad . \tag{38}$$

In the absence of a space charge region, that is, when $v_s = 0$, the filament conductance would be given by

$$g_b = \frac{\sigma_b (d_s + d_b)w}{\ell} \quad . \tag{39}$$

Hence, the change in conductance, parallel to the surface, when v_s is changed from 0 to v_s is

$$\Delta g = g - g_b$$

$$= \frac{(\sigma_s - \sigma_b)d_s w}{\ell} \quad . \tag{40}$$

The surface conductance per square surface area ΔG is now defined as

$$\Delta G = \frac{\ell}{w} \Delta g$$

$$= (\sigma_s - \sigma_b)d_s \quad . \tag{41}$$

Since both ℓ and w have the dimensions of length, ΔG has the dimensions of conductance. However, ΔG does not represent the total conductance of the filament. ΔG is called the surface

conductance per square and its units are usually written as mhos/sq. or μmhos/sq. ΔG will be the same for a square area of the surface whether it be a square cm. or a square meter or any other unit of area.

In order to evaluate ΔG as a function of v_s and u_b, we need to evaluate σ_s and σ_b. From the fundamental equation

$$\sigma = q(\mu_n n + \mu_p p) , \tag{42}$$

we can write

$$\sigma_b = q(\mu_n n_b + \mu_p p_b). \tag{43}$$

Since σ_s is the average conductivity of the space charge region, it can be written as

$$\sigma_s = \frac{1}{d_s} \int_0^{d_s} \sigma(x)dx$$

$$\sigma_s = \frac{1}{d_s} \int_0^{d_s} q(\mu_n n(x) + \mu_p p(x))dx . \tag{44}$$

If we assume that the hole and electron mobilities in the space charge region are the same as in the bulk, which is a fair assumption except in the case of strong accumulation or inversion regions,[16] then using (41), (43) and (44), and the fact that σ_b is a constant and can be taken under the integral sign, we have

$$\Delta G = \int_0^{d_s} [q\mu_n(n-n_b) + q\mu_p(p-p_b)]dx$$

$$= \int_0^{d_s} q\mu_n(n-n_b)dx + \int_0^{d_s} q\mu_p(p-p_b)dx \quad . \qquad (45)$$

We now note that for the upper limit of the integrals, d_s can be replaced by ∞, since in reality the space charge region approaches the bulk conditions only asymptotically.

Hence, we have

$$\Delta G = q(\mu_n \Delta N + \mu_p \Delta P) \quad , \qquad (46)$$

where ΔN, ΔP are the excess surface carrier densities given by (35) and (36). This equation tells us that ΔG, like Σ_{sc}, is also a single valued function of v_s for a given u_b so that theoretical curves of ΔG versus v_s can be plotted for a wide range of values of v_s. Also, it is possible to plot ΔG versus Σ_{sc} with v_s as a parameter. As will be shown, such a theoretical $\Delta G - \Sigma_{sc}$ curve is at the very basis of interpreting data from ac field effect measurements.

Theoretical ΔG versus Σ_{sc} Curve

Fig. 5 shows a theoretical curve of ΔG versus Σ_{sc} for 450 ohm-cm n-type silicon. ($u_b = 6.676$ and $L = 1.23$ microns). The values of the surface potential v_s are also indicated on the

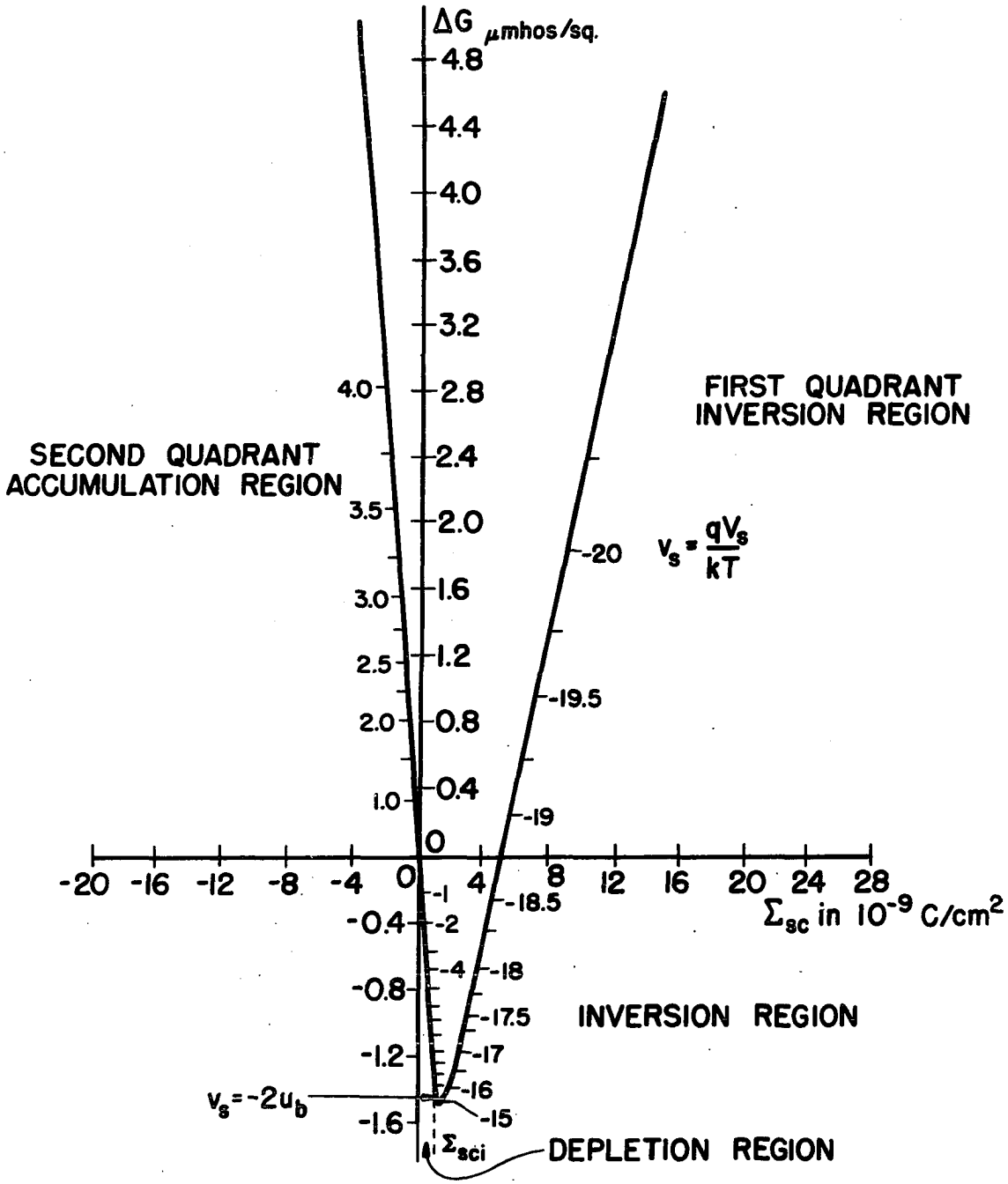

FIG. 5 THEORETICAL $\Delta G - \Sigma_{SC}$ CURVE

curve. This curve was obtained by evaluating the integrals for ΔN and ΔP numerically on an IBM 360 Model 40 digital computer using the 36-point Gauss-Legendre Quadrature method. ΔN and ΔP were evaluated for values of v_s ranging from -25 to +25 in steps of 0.25, corresponding to the bending of the energy bands by 0.65 eV in either direction around flatbands, in steps of 0.0065 eV.

Starting with v_s large and positive, we can trace through three distinct regions of the curve as v_s goes through zero to large negative values.

The region $\Delta G > 0$, $\Sigma_{sc} < 0$, $(v_s > 0)$ corresponds to an accumulation region. The space charge is negative, the bands bend down and the surface conductance is mainly due to the large number of majority carriers (electrons for n-type). As v_s approaches zero through positive values, ΔN reduces but ΔP does not increase significantly so that ΔG reduces, as does $|\Sigma_{sc}|$. At $v_s = 0$, we have flatbands and both ΔG and Σ_{sc} must be zero by definition. The curve thus passes through the origin at flatbands.

The region $\Delta G < 0$, $\Sigma_{sci} > \Sigma_{sc} > 0$ $(-2u_b < v_s < 0)$ corresponds to the depletion region. As v_s becomes negative, the bands bend up and the space charge becomes positive. ΔN continues to decrease but the increase in ΔP is not sufficient to contribute significantly to the surface conductance so that ΔG keeps on decreasing. At $v_s = -2u_b$, the free hole density at the surface becomes equal to the bulk electron density and we enter into the inversion region.

For $\Sigma_{sc} > \Sigma_{sci} > 0$ ($v_s < -2u_b$) we have the inversion region. For $v_s < -2u_b$, ΔG continues to reduce further until at

$$v_s = -2u_b - \ln(\mu_n/\mu_p) \quad . \tag{47}$$

ΔG reaches a minimum value. It is seen that the surface potential at which the conductance minimum occurs is a unique function of u_b and is approximately equal to $-2u_b$ for large u_b.

As v_s becomes more negative beyond the conductance minimum, ΔG starts increasing due to hole conduction. The curve once again passes through $\Delta G = 0$ when

$$\frac{\Delta N}{\Delta P} = -\frac{\mu_p}{\mu_n} \quad . \tag{48}$$

Beyond that point, we have a strong inversion layer and the surface conductance is due mainly to minority carriers (holes in this case).

It may be noted that the ΔG versus Σ_{sc} curve is linear over most part except near the conductance minimum and at very large values of v_s where saturation effects and degeneracy set in.

No corrections have been applied in evaluating the theoretical ΔG v/s Σ_{sc} curve for the reduction of mobilities of electrons and holes in the space charge region due to surface scattering. Such corrections, first worked out by Schrieffer,[28] are important only for strong accumulation and inversion layers, that is, large values of v_s. Since such large $|v_s|$ values are ordinarily unrealizable in practice, Schrieffer's corrections are generally neglected.[8]

Surface States

A brief discussion on surface states was presented in Chapter 1. It was mentioned there that surface states can be of the fast or slow type and can also be donor-like or acceptor-like. We will now discuss in some detail the origin and nature of both slow and fast states and the effects of donor- and acceptor-like states on the energy band structure of a semiconductor near its surface.

Consider the energy level diagram for an n-type semiconductor as shown in Fig. 6a. When there are no surface states present, and in the absence of an external electric field, flatband conditions will exist. Now suppose that acceptor-like surface states with a density N_t per cm^2, regardless of being of the fast or slow type, are introduced at an energy level E_t below the Fermi level. Since the surface states are empty and below the Fermi level, some of the electrons from the conduction band will fall into them. This causes a sheet of negative charge at the surface and a positive space charge underneath it. The energy bands in the space charge region will bend upwards with respect to the Fermi level. Also, since the localized levels E_t are due to short range atomic forces (micropotential) and are hence unaffected by the space charge macropotential, they will ride with the energy bands. Equilibrium will be reached when the positive space charge is exactly equal in magnitude to the negative surface states charge. Under equilibrium,

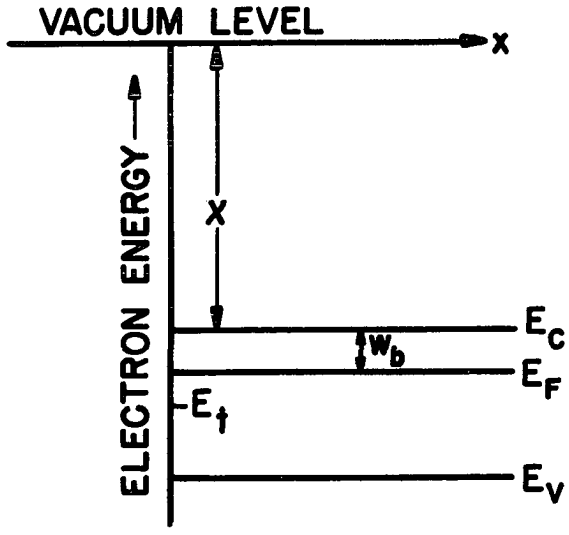

Fig. 6a Energy Band Diagram Just After Introduction of N_t cm^{-2} Acceptor-like Surface States at Energy E_t

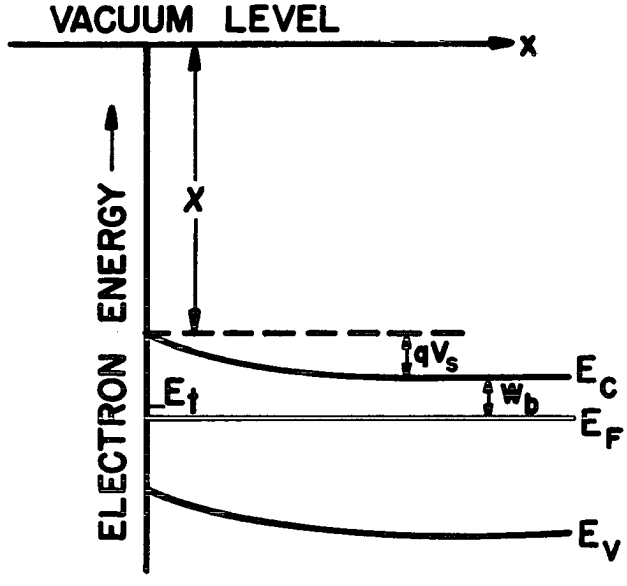

Fig. 6b Energy Band Diagram of (a) After Reaching Thermal Equilibrium

Fig. 6

Effect of Acceptor-like Surface States on the Energy Bands of n-type Silicon

the levels E_t will lie slightly above the Fermi level and will therefore be only partially filled. The equilibrium condition is shown in Fig. 6b.

We have thus seen that the presence of acceptor-like states at the surface bends the energy bands upwards and gives rise to a positive space charge. This statement is obviously true even for a p-type semiconductor. An argument similar to the one above will show that when donor-like surface states are introduced above the Fermi level, holes from the valence band will fall into them and the energy bands of both p- and n-type semiconductors will bend downwards, leading to a negative space charge.

Thus, for an n-type semiconductor, donor-like surface states will give rise to an accumulation region and acceptor-like states will cause a depletion region and, perhaps an inversion region also. Also, the larger the number of ionized surface states, the greater the magnitude of the surface sheet of charge and the more the bending of the energy bands.

Normally, on a real surface of a semiconductor, that is, on a surface that is chemically etched and exposed to the atmosphere or other gases, there exist both donor- and acceptor-like surface states simultaneously. The bending of the energy bands and the type of space charge will then be due to the overall net effect of both kinds of states. It is then possible that on the same piece of a semiconductor, there may be different regions of the surface with differing space charge. In contrast to this, a clean surface,

such as is obtained by cleavage under ultra-high vacuum or by ion bombardment and annealing, is always found to have a positive space charge, corresponding to acceptor-like surface states, on both n- and p-type semiconductors. This is believed to be due to electrons trapped by the dangling bonds at the surface.

The charge carriers which are trapped in surface states behave as bound charges and do not take part in the conduction process under normal electric fields. This, of course, is for the same reason that charge carriers in donor and acceptor impurity levels behave like bound charges. However, as will be pointed out later, charge trapped in slow surface states will migrate extremely slowly on the surface under the influence of an electric field parallel to the surface. The current due to such a surface ionic migration is negligible but it does give rise to a significant variation of the depletion width and reverse junction capacitance of metal-semiconductor surface barriers over a period of minutes or hours.

The occupation statistics of surface states is governed by the Fermi-Dirac statistics in the same manner as for impurity levels. Thus, the probability that an electron occupies the energy level E_t is[30]

$$f_n(E_t) = \frac{1}{1+\frac{g_o}{g_i}\exp\left[(E_t - E_F)/kT\right]} , \qquad (49)$$

where g_o and g_i represent the number of degenerate quantum

states of the level E_t when it is vacant and occupied, respectively. If we now define an effective energy level E_t^f such that

$$E_t^f = E_t + kT \ln(g_o/g_i) \ , \tag{50}$$

then the occupation probability can be written[16] as

$$f_n(E_t^f) = \frac{1}{1 + \exp\left[(E_t^f - E_F)/kT\right]} \ . \tag{51}$$

The surface densities of occupied and unoccupied surface levels will be given by

$$n_t = N_t \, f_n(E_t^f) \tag{52}$$

$$p_t = N_t \, f_p(E_t^f) \ , \tag{53}$$

where $f_p(E_t^f) = 1 - f_n(E_t^f)$ and $n_t + p_t = N_t$ is the total density of surface levels at the energy E_t. The surface levels will now be half occupied when the Fermi level coincides with E_t^f rather than with E_t. The maximum rate of variation of $f_n(E_t^f)$ and $f_p(E_t^f)$ with energy occurs at $E_t^f = E_F$. Hence, surface states close to the Fermi level are the most effective. Those close to the band edges are the least effective. Of course, E_t^f also rides with the energy bands so that the occupation probability changes as the bands bend.

In general, there can be several surface state energy levels. The net surface charge density can then be given by

$$\Sigma_{ss} = q \sum_j N_{tj} f_p(E^f_{tj}) - q \sum_k N_{tk} f_n(E^f_{tk}) \quad , \qquad (54)$$

where N_{tj} is the surface density of donor-like levels at energy E_{tj} and N_{tk} is the surface density of acceptor-like levels at energy E_{tk}.

In the absence of an external electric field, there will be a space charge of equal magnitude and opposite polarity, so that the total charge density Σ_T is given by

$$\Sigma_T = \Sigma_{ss} + \Sigma_{sc} = 0 \quad . \qquad (55)$$

If an externally applied electric field exists at the surface, (such as, for example, a capacitively applied field), then the charge induced by the applied field will be divided between the surface charge (charge bound in surface states) and the space charge. Gauss' law will then give

$$\Sigma_a + \Sigma_T = 0 \quad , \qquad (56)$$

where

$$\Sigma_a = \pm D_a = \pm \varepsilon_i \varepsilon_o E_a \quad . \qquad (57)$$

D_a is the magnitude of the electric displacement vector and ε_i is the dielectric constant of the medium external to the semiconductor surface. E_a is the electric field strength in this surrounding medium. The plus sign is for the electric field pointing into the

semiconductor surface and the minus sign is for the field pointing outwards. For the case of an applied electric field, we then have

$$\Sigma_T = \Sigma_{ss} + \Sigma_{sc} = -\Sigma_a \quad . \tag{58}$$

So far, it has not been necessary to distinguish between fast and slow surface states. However, such a distinction becomes essential when considering the effects of a time varying external electric field. Actually, the distinction is more fundamental than that of merely differing transient behavior. The nature and origin of fast and slow states are quite different, and they behave quite differently under different physical and chemical conditions. Hence a brief description of the origin and nature of fast and slow surface states will be presented after defining them in terms of their transient behavior.

Consider a capacitor made up of a metal electrode in the close proximity of an n-type semiconductor surface with an intervening dielectric medium. This is shown in Fig. 7a. Suppose that this capacitor is uncharged at first and a net density of acceptor-like surface states causes the energy bands to bend upwards as in Fig. 7b. If now the metal electrode is given a negative potential with respect to the semiconductor, then the electric field in the dielectric will be pointing outwards from the semiconductor surface. The capacitor charges up by removing some of the free electrons from the space charge region of the semiconductor, thereby bending the energy bands still further upwards.

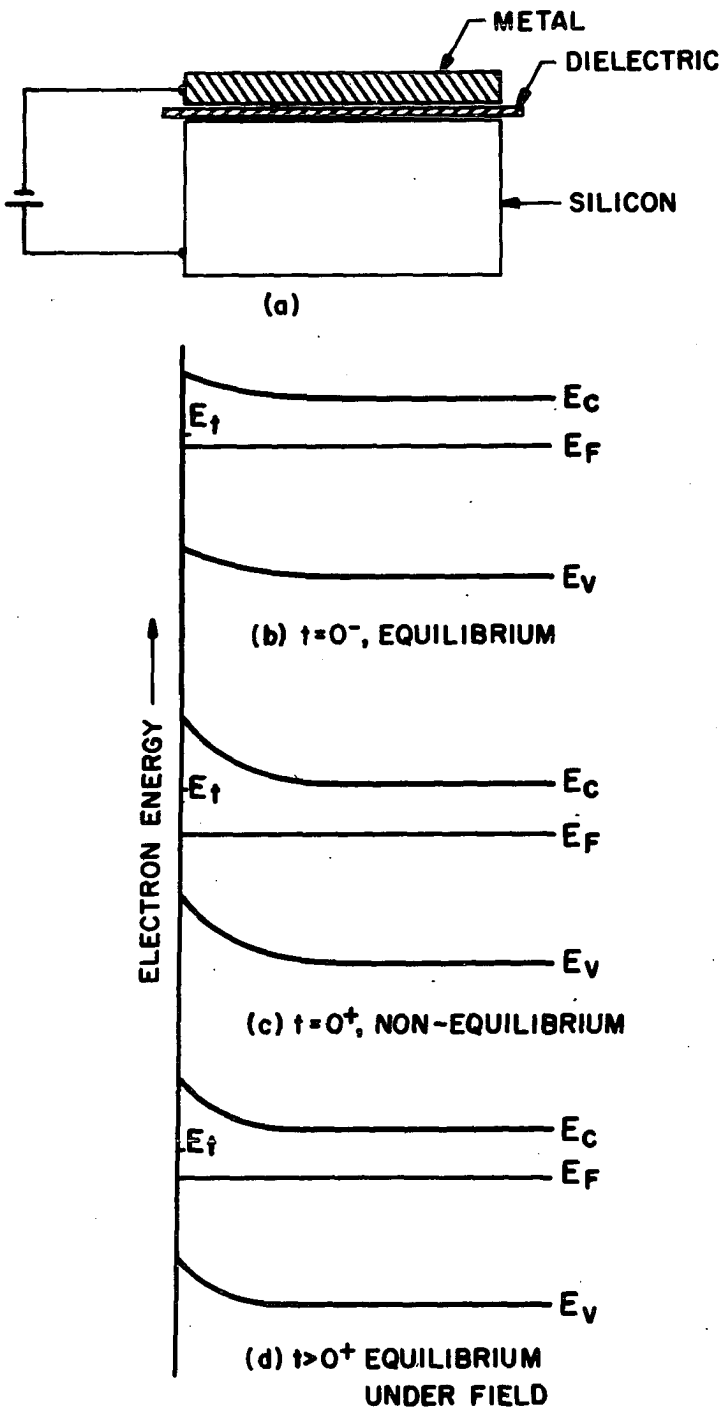

Fig. 7 Transient Behavior of Surface States

It is assumed, for simplicity, that the surface potential v_s is not too large even in the presence of the electric field so that the minority carrier (hole) density in the space charge region is still negligible. This assumption is very often justified in practice. This charging up process takes place in a relatively short time (of the order of 10^{-8} sec or less) so that the conduction band of the semiconductor is in equilibrium with the field within this short time after the application of the field. The energy band diagram at this instant $(t = 0^+)$ is shown in Fig. 7c. The surface states are still not in equilibrium with the induced charge. This equilibrium can be reached only when some of the electrons are released from the acceptor-like surface states into the conduction band and when the conditions of (54) and (58) are both satisfied. The final equilibrium conditions are shown in Fig. 7d. As the equilibrium between the surface states and the induced charge is being reached, the energy bands will relax towards their original pre-field positions. The amount of relaxation is determined by the densities and energy positions of the surface states. Hence, a study of the transient behavior of surface states can yield information regarding their densities and energy positions.

The induced charge is distributed between the space charge and the surface charge. Effectively, then, the surface states partially shield the space charge from an external field. With a high density of surface states close to the Fermi level, the shielding or relaxation can be almost total.

The fast and slow surface states are defined with respect to their relaxation times, that is, the time they require to reach equilibrium with the induced charge. Those surface states which have a relaxation time of the order of 10^{-5} sec. or less are called fast surface states. Surface states with a relaxation time ranging from about 10^{-2} sec. to several hours are called slow states.

We can now discuss the origin and nature of fast and slow surface states. Considering the fast states first, it is reasonable to assume that since the fast states do not require too much time to come into equilibrium with the energy bands, they must have an intimate contact with the semiconductor surface. The fast states are therefore assumed to exist at the semiconductor surface itself.

It was first shown by Tamm,[12] and later by Shockley,[13] that even at an ideal surface (free of defects, impurities, adsorbed atoms or displacement of surface atoms), localized energy levels can exist with a density of roughly one per surface atom, due to the termination of the crystal lattice. More crudely, we can say that dangling bonds of the surface atoms will exist at the surface and that electrons can be trapped to satisfy these dangling bonds. The actual structure of a semiconductor surface is rather complex but it has been observed in practice that a clean semiconductor surface always has a positive space-charge which confirms the dangling bond hypothesis to some extent. In reality, there will be impurities (dopant) and defects even on a clean surface and these can give rise to fast surface states also. It is customary to associate

fast surface states to surface trapping and recombination levels, regardless of the origin of such trapping levels. Electrically, the behavior of these surface levels is the same as that of trapping and recombination centers in the bulk.

Fast surface states will also exist on chemically etched (real) surfaces which are exposed to the atmosphere. The density of fast states on real surfaces is found to be about two to three orders of magnitude smaller than on clean surfaces. This is believed to be due to the satisfaction of some of the dangling bonds by adsorbed atoms. Both chemical surface treatments (etching, quenching, and post-etch chemical treatments) and gaseous ambients affect the densities of fast surface states. There is experimental evidence that the energy positions of the fast states are quite insensitive to chemical surface treatments and gaseous ambients.[16] This evidence is quite conclusive for the case of gaseous ambients but not so conclusive for chemical surface treatments.

The slow surface states are usually associated with chemisorbed atoms. A real semiconductor surface will normally have a layer of chemisorbed atoms on it and such atoms can also trap electrons or holes. Since these trapping levels do not have an intimate contact with the semiconductor surface, their relaxation times will be comparatively large. The presence of the slow surface states will affect the densities of fast states in two ways. First, the slow states can satisfy some of the dangling bonds. Secondly, the charge trapped in the slow states will cause an equal

and opposite charge to be distributed between the fast states and the space charge. The bending of the energy bands will therefore change, thereby changing the occupation densities of the fast states. Thus, we note that gaseous ambients can change the surface potential in much the same manner as an applied external electric field. Actually, different gases and vapors can change the surface potential much more effectively than an electric field. Coupled with their lack of influence on the energy positions of fast states, this makes them very useful in ac field effect measurements.

Theory of the Low Frequency AC Field Effect

Consider an n-type silicon surface under a given ambient in the absence of an external electric field. Gauss' law then gives

$$\Sigma_{sss} + \Sigma_{fss} + \Sigma_{sc} = 0 \quad , \tag{59}$$

where Σ_{sss} and Σ_{fss} are the surface charge densities in the slow and fast surface states respectively. Under an external electric field corresponding to an inducing charge density Σ_a, we have

$$\Sigma_{fss} + \Sigma_{sc} = -(\Sigma_{sss} + \Sigma_a) = \Sigma_{in} \quad , \tag{60}$$

where Σ_{in} is the charge density induced by the combined action of ionized slow surface states and an electric field.

Now suppose that the external electric field is an ac field with a frequency which is high enough so as to prevent

the interaction of the slow surface states with the induced charge but low enough to allow complete interaction between the fast surface states and the induced charge. Such a frequency can lie between a few Hz and a few KHz. Then, if $\Delta\Sigma_a$ represents the change in Σ_a over a time Δt, we will have

$$\Delta\Sigma_{fss} + \Delta\Sigma_{sc} = -\Delta\Sigma_a = \Delta\Sigma_{in} \tag{61}$$

that is, the induced charge is distributed only between the fast states and the space charge. Now the charge trapped in the fast surface states, Σ_{fss}, is immobile and therefore does not contribute to the surface conductance. Also, the charge Σ_{fss}, being at the very surface, does not enter into Poisson's equation (Eq. (24)) for the relation between Σ_{sc} and v_s. Even in the presence of Σ_{fss}, the surface potential v_s is still a single-valued function of Σ_{sc} (v_s is a double-valued function of ΔG although ΔG is a single-valued function of v_s but in the case of Σ_{sc} and v_s, each is a single-valued function of the other). Thus we see that the fraction of the induced charge which goes into the space-charge region, namely $\Delta\Sigma_{sc}$, gives rise to a unique change in the surface potential v_s, which, in turn, gives rise to a unique change in the surface conductance. What happens in practice is that a given ambient (Σ_{sss}) determines a definite surface potential v_s, and hence, definite values of Σ_{sc} and ΔG, in the absence of an electric field. An ac electric field then varies v_s, Σ_{sc} and ΔG by small amounts around their equilibrium field-free values.

Another ambient allows different field-free values of v_s , Σ_{sc} and ΔG around which they can be varied by the applied electric field. By using a sufficient number of different ambients, it is possible, in principle, to cover a large range of values of v_s , Σ_{sc} and ΔG . Thus, it is possible to cover a significant portion of the theoretical ΔG versus Σ_{sc} curve, including the conductance minimum. The different ambients affect only the occupation densities of fast surface states but not their energy positions in the forbidden band. This allows the field effect curves for different ambients to partially overlap and to form a smooth overall curve which would otherwise be obtained with a single ambient and a large enough ac electric field. Thus, the different ambients perform the same function as would an unrealizably large applied electric field.

The experimental field effect curve is built up of a number of field effect curves, each of which depicts the change in surface conductance from its field-free value versus the total field-induced charge density $\Delta\Sigma_{in} = \Delta\Sigma_{fss} + \Delta\Sigma_{sc}$. $\Delta\Sigma_{in}$ can be calculated from the known magnitude of the applied ac field using (57). If the overall experimental curve contains the conductance minimum, then we know that the conductance minimum should occur at the same value of v_s and Σ_{sc} as for the theoretical curve. We therefore align the theoretical and the experimental curves so that their conductance minima coincide along the surface conductance axis. Then the ordinates of the experimental curve will also

represent the true values of ΔG. Also, the values of v_s and Σ_{sc} for each point on the experimental curve will be the same as for a corresponding point on the theoretical curve. A corresponding point on the theoretical curve is one which has the same value of ΔG and which lies in the same type of region (accumulation, depletion, or inversion) as the chosen point on the experimental curve. Although v_s is a double valued function of ΔG, if the type of region is also specified along with ΔG, then a unique relation between v_s and ΔG can be established.

The abscissa on the overall experimental field effect curve will be $\Sigma_{in} = \Sigma_{fss} + \Sigma_{sc}$, except that no precise reference point is available along this axis as it is along the ΔG axis. This is because the charge induced by any given ambient is not known in absolute magnitude. If the reference point for the induced charge is arbitrarily chosen to correspond to zero electric field in some specific ambient such as vacuum or oxygen, then the conductance minimum of the theoretical curve can be aligned with that reference point on the experimental curve. The difference along the abscissa between two corresponding points on the experimental and theoretical curves will then give Σ_{fss}, the surface density of charge trapped in fast surface states with respect to its value under the reference ambient. Of course, the value of Σ_{fss} for any ambient will be in error by at most an additive constant. The field effect measurements are still useful in yielding the correct order of magnitude of the density of ionized

fast states. The densities for different ambients in reference to the chosen standard ambient will not suffer from any error other than due to the limits of experimental accuracy.

We have thus seen that by measuring the surface conductance modulation under a capacitively applied transverse ac electric field, it is possible to evaluate the surface potential v_s and the density of ionized fast states for different ambients, provided that the conductance minimum can be experimentally achieved. From the variation of the occupation densities of fast states with v_s, it is also possible to evaluate the energy levels of the fast states. However, this cannot be done uniquely since several different sets of energy levels will give rise to the same occupation statistics. Hence, no effort was made in this work to evaluate the energy levels of fast surface states. The greatest utility of the field effect technique lies in the fact that it enables one to quite accurately measure the influence of chemical surface treatments and gaseous ambients on the surface potential and the density of fast surface states at a semiconductor surface. The relative simplicity of this method together with its versatility has made it by far the most popular technique in the study of semiconductor surfaces.

The Au-n-Si Surface Barrier in the Presence of Surface States

We have seen that a metal semiconductor contact in the absence of surface states will behave according to the Schottky theory

and will have no surface channel conductance. The difference between the metal and semiconductor work functions causes a surface potential barrier and a space charge to appear under the semiconductor surface and the contact exhibits electrical rectification characteristics.

In the presence of surface states, a potential barrier will normally exist at the semiconductor surface even without a metal contact. If now a contact is made with a metal, then most of the induced charge due to the electric field arising out of the work function difference will lie in the surface states rather than in the space charge. For the specific case of the Au-n-Si contact, the silicon energy bands under the gold contact will bend upwards by only a small amount compared to the bending in the absence of surface states. The surface states thus effectively shield the semiconductor space charge region from an external electric field. The larger the density of surface states and the closer their energy positions to the Fermi level, the more effective is their shielding. Figures 8a and b show, respectively, the energy band diagrams of an n-type silicon surface with acceptor-like surface states before and after contact with gold.

It is seen from the above discussion that in the presence of a large density of surface states, the barrier height of the metal-semiconductor contact will show little or no relation to the metal-semiconductor work function differences. This means that the recitfication characteristics of a metal-semiconductor contact

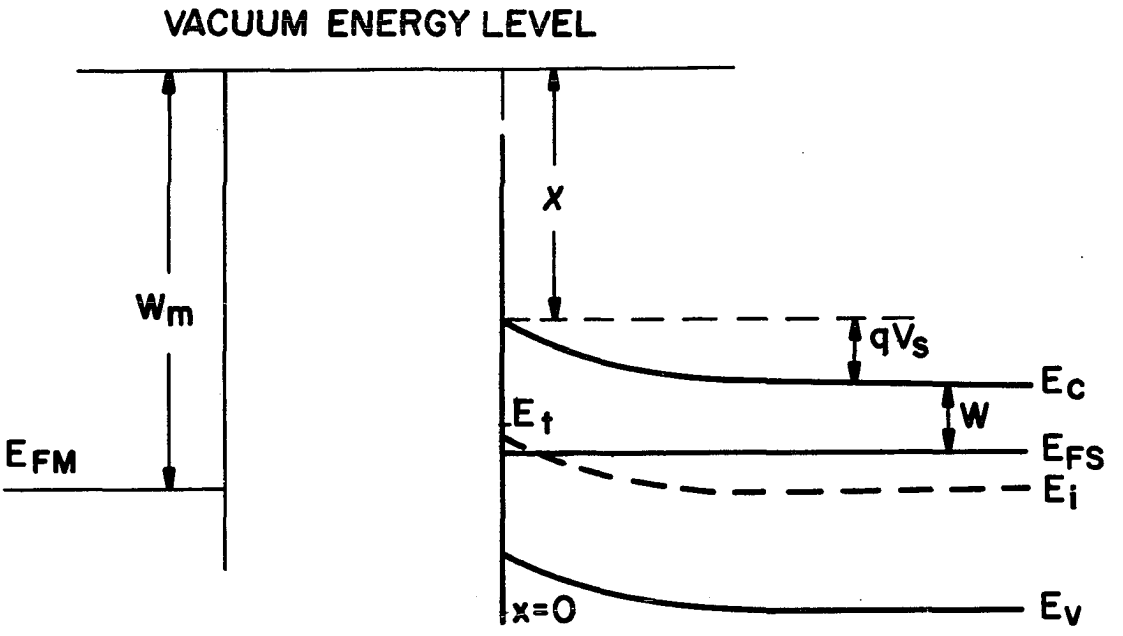

Fig. 8a Energy Band Diagrams of the Metal and Semiconductor Before Contact, in the Presence of Acceptor-like Surface States

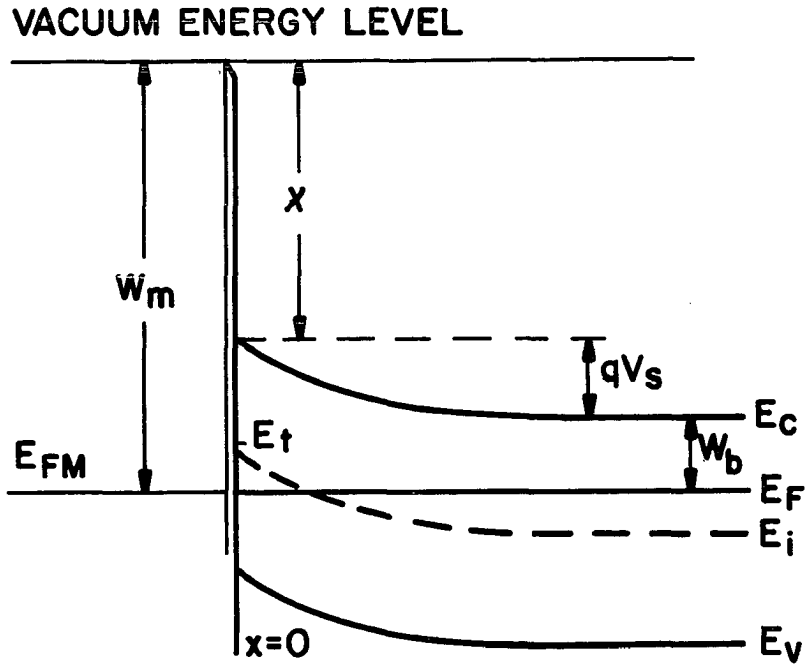

Fig. 8b Energy Band Diagrams of the Metal and Semiconductor After Contact and in Thermal Equilibrium. Surface States Shield the Semiconductor Space Charge

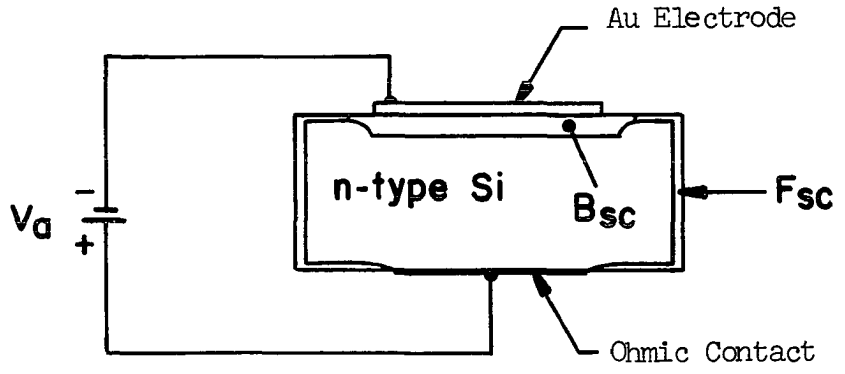

Fig. 8c Au-n-Si Surface Barrier in the Presence of Surface States

can be controlled more by the surface treatments and ambients than by the type of metal used. This explains the experimental observation that after sufficient exposure to air, almost any metal yields a rectifying contact on n-type silicon regardless of its work function.

However, the metal work function does play an important role in yielding low reverse current surface barriers. The role of the metal can only be appreciated after considering the reverse current-voltage characteristic.

Consider the Au-n-Si surface barrier as shown in Fig. 8c. A relatively large net density of acceptor-like surface states is assumed to be present on the entire silicon surface. Let B_{sc} and F_{sc} denote the space charge regions under the gold electrode and under the free surface respectively. The corresponding surface potentials will be V_d and V_s. Now V_d and V_s will in general be different. The causes for their difference will be discussed later. Here, we need only consider the consequences of their difference. We may recall that V_d and V_s will uniquely determine the excess carrier concentrations ΔN and ΔP in the two regions. Thus, if V_d and V_s are different from each other, a graded junction will be formed between B_{sc} and F_{sc}.

Now consider the application of a reverse voltage to this surface barrier rectifier. First of all, there will be a reverse current through B_{sc}. There is sufficient experimental evidence to show that this reverse current does not depend directly on V_d as

predicted by the Schottky theory. Rather, it is made up of the bulk diffusion and the space-charge generation currents as given by (10) and (11), just as for a regular p-n junction diode. In fact, except for the surface channel current, the surface barrier diode behaves exactly like a one-sided step p-n junction. The V_d of the surface barrier corresponds to the built-in voltage of the p-n junction except that whereas the latter depends on the product of the impurity doping concentrations in each region, the former depends on the silicon doping concetration, the densities and energy positions of surface states and on the metal work function in a rather complex manner.[22]

Next, we must consider the current that flows across the boundary between B_{sc} and F_{sc} and through F_{sc} to the bulk contact. Three possible cases can be considered for this current.

(1) If $|V_s| > |V_d|$, then ΔP will be larger in F_{sc} than in B_{sc} and the B_{sc}- F_{sc} junction will be forward biased since F_{sc} is at a positive potential with respect to B_{sc}. A large space-charge-limited channel current will now flow so that the overall reverse current will be predominantly made up of this channel current.

(2) If $|V_s| = |V_d|$, then again a large space-charge-limited channel current will flow of approximately the same magnitude as in the first case.

(3) If $|V_s| < |V_d|$, then the B_{sc}- F_{sc} junction will

be reverse biased and the channel current will be the small reverse current through the B_{sc}- F_{sc} junction as long as the reverse voltage across this junction is much smaller than its avalanche breakdown voltage.

In reality, the B_{sc}- F_{sc} junction will be a two-dimensional graded junction and the development of its exact theory is extremely difficult. However, we can see from the above arguments that the reverse current of a surface barrier will depend on both V_d and V_s and not on V_d alone. Also, it is because of this reason that the reverse characteristics are so much dependent on surface treatments, quenchants, ambients and the metal work function since all of these factors control V_d and the first three control V_s . Also, it is possible that the breakdown voltage of the B_{sc}- F_{sc} junction may be significantly lower than that of the Au-Si contact either due to strong accumulation or inversion of the free surface, or due to localized inhomogeneities of the surface states charge or both. This may therefore control the overall breakdown voltage of the surface barrier.

In order to investigate the effects of surface treatments, etchants and quenchants on the rectification characteristics of the Au-n-Si surface barrier, it is therefore necessary to study the variation of both V_d and V_s with each of these variables. Of these two, V_d can be evaluated by differential capacitance measurements on a surface barrier. However, V_s must be evaluated by low frequency field effect measurements on filamentary samples

prepared in the same manner as the surface barrier except for the gold evaporation.

We can now see why the metal work function does play a secondary yet important role in controlling the rectification characteristic of a surface barrier. If the metal work function is larger than that of the n-type silicon, then the electric field resulting from the work function difference will aid the fixation of negative ions such as O^-. It will thereby help create an inversion layer under the gold electrode. The strength of inversion may be controlled by the surface treatment and quenchant (density of fast surface states). Thus, a metal such as Au or Pt exhibits good rectification characteristics within minutes or hours after exposure to air, whereas low work function metals require several months of exposure to air. Even then they do not yield such low reverse currents as are obtained with Au, Pt, Cr etc.

CHAPTER IV

EXPERIMENTAL WORK ON Au-n-Si SURFACE BARRIERS

Fabrication

In order to investigate the effects of etch quenchants and post-etch chemical surface treatments on the rectification properties of Au-n-Si surface barriers, different combinations of these were used in the fabrication procedures.

The choice of the different quenchants investigated was based on the following reasoning. Since the active components of the etchant CP4A are HNO_3 and HF, it was argued that if an excess of HNO_3 gives rise to a thin stain film on the silicon surface, then an excess of HF would give rise to a thick film compared to that given by deionized water. Thus, the three different quenchants chosen were: (1) excess HF, (2) deionized water and (3) excess HNO_3 .

The post-etch surface treatments used were: (1) no specific chemical but storage in deionized water for 1-2 weeks with water changed daily, (2) immersion in boiling deionized water for 30-40 min, (3) immersion in 1% aqueous solution of potassium dichromate at 70-80°C for 20-30 min and (4) immersion in aqua regia (HCL/HNO_3 = 3/1) at 70-80° for 20 min. The first treatment was

found by Reynolds and Persson[18] to yield low reverse current diodes. However, their treatment also included a two week exposure to filtered air prior to gold evaporation which was not used in this work. The boiling water and sodium dichromate treatments have been widely used except that potassium dichromate was used instead of sodium dichromate, since it is a very strong oxidizing agent. The aqua regia treatment evolved from an observation that surface barriers which were once fabricated and destroyed by dissolving the gold electrode in aqua regia turned out to be better rectifiers upon refabrication, in spite of a thorough rinsing in deionized water and re-etching.

Pre-etch Preparation

Several 5 mm thick slices were cut from a single 450 ohm-cm n-type silicon ingot of 2 cm diameter and with the axis along the (111) crystallographic direction. The minority carrier lifetime was unknown but based on the reverse currents it was calculated to be of the order of 100 μsec. These slices were once made into Au-Si surface barriers but were found to have poor reverse characteristics. The detectors were therefore destroyed by immersion in hot aqua regia.

Each slice was then lapped on both faces with American Optical M302, M303 abrasives on a ground glass plate. After rinsing away the abrasive, they were then given an ultrasonic detergent bath, rinsed with deionized water, given an ultrasonic bath in TCE

(trichloroethylene), dried on filter paper and stored in deionized water in a very thoroughly rinsed beaker. After lapping, each slice was handled exclusively with a set of clean teflon coated tweezers.

Etching and Quenching

The etchant used was CP4A which is made up of HNO_3: HF: CH_3COOH = 5:3:3. Fresh etchant was made each day and was cooled for 2-4 hours in ice before use. Each slice was individually etched in about 120 ml. of etchant for 24 minutes with the etching beaker being surrounded by ice-cold water and being stirred quite vigorously by hand. The etching action was quenched in one of the following three manners.

1. After 24 min. of etching, about 50 ml of concentrated (48%) HF was added to the etchant and stirred for another 10-15 seconds after which deionized water was gradually added and the flushing or rinsing was performed until the resistivity of the overflowing water was about 1 Megohm-cm.

2. The etching was quenched by high resistivity deionized water followed by a thorough rinsing in deionized water.

3. Same as in the case of HF quenching except that the quenchant was about 100 ml. of concentrated (70%) HNO_3.

Surface Treatments

Following quenching and rinsing, the silicon slice was

given one of the four chemical surface treatments described above.

A light rinse in deionized water was given after each surface treatment except the first. Care was taken to minimize exposure to air from the start of etching till the completion of the gold evaporation. Thus, after the surface treatments, the slices were again stored in deionized water for 1-2 days until ready for gold evaporation.

Gold Evaporation and Contacts

A gold electrode of 12.5 mm in diameter and 20 $\mu gm/cm^2$ thickness was evaporated on each crystal through teflon masks. A 2.5 mm diameter gold dot of additional thickness was evaporated at the periphery of each gold electrode for making contact to it. The back contact was made with Anchor Alloy model Shurbond III conducting silver paste. To ensure a good non-rectifying contact, a 2-3 mm diameter area of the back face of each crystal was lightly scratched with a diamond point prior to gold evaporation. After gold evaporation, the crystal was mounted on a 7 mm diameter kovar stud covered with silver paste. The overall mounting arrangement is shown in Fig. 9. Contact with the gold electrode was made by bonding a gold band onto the thick gold dot with silver paste. The completed surface barriers were stored in a clean dust-free enclosure. No form of edge-protection or encapsulation was used.

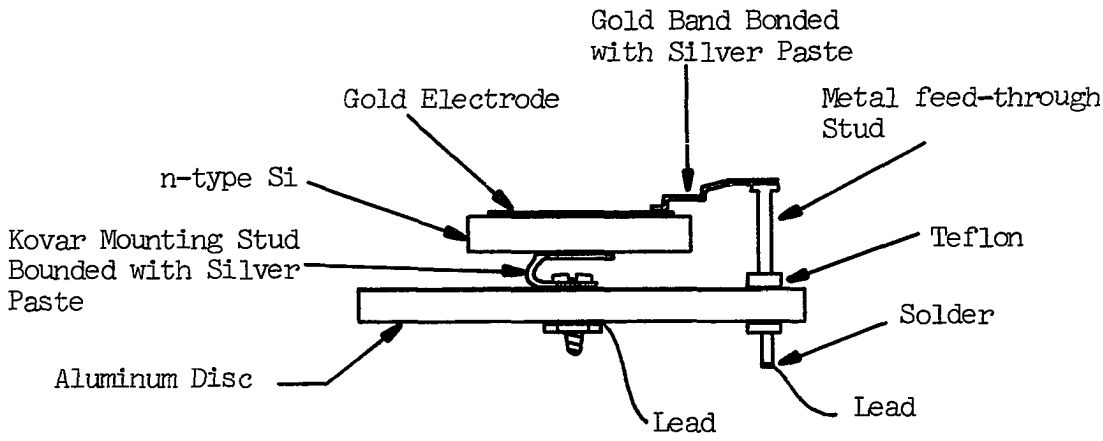

Fig. 9 Mounting Arrangement of the Au-n-Si Surface Barrier

Quenchant / Surface Treatment	HF	H_2O	HNO_3
Storage in deionized H_2O	NOH	NOW	NON
Aqua Regia	ARH	ARW	ARN
Boiling Water	BWH	BWW	BWN
Potassium dichromate	DIH	DIW	DIN

Identification Scheme

Table 1 shows the scheme of names used to identify each surface barrier.

The first two letters of each name identifies the surface treatment - AR for aqua regia, DI for dichromate, etc., and the last letter identifies the quenchant used - H for hydrofluoric acid, W for water and N for nitric acid. This system of naming has an advantage over a numbering scheme in the fact that during the discussion of the comparative properties of different surface treatments and quenchants, one need not refer back or commit to memory the correspondence between a number and the method of preparation.

The surface barrier NOW was not prepared since it had been studied extensively prior to this work. However, field effect measurements were also performed on an NOW sample.

Reverse Current-Voltage Characteristics

Both forward and reverse current-voltage characteristics were measured on a Tektronix Model 575 transistor curve tracer at several intervals of time over a seven month period. Figures 10 and 11 show the curve tracer photographs taken after storage in filtered room air for one week and seven months respectively. For both forward and reverse polarities, the scale along the voltage (horizontal) axis is 20 volts/cm. and that along the current (vertical) axis is 100 μA/cm. The hysterisis in the reverse

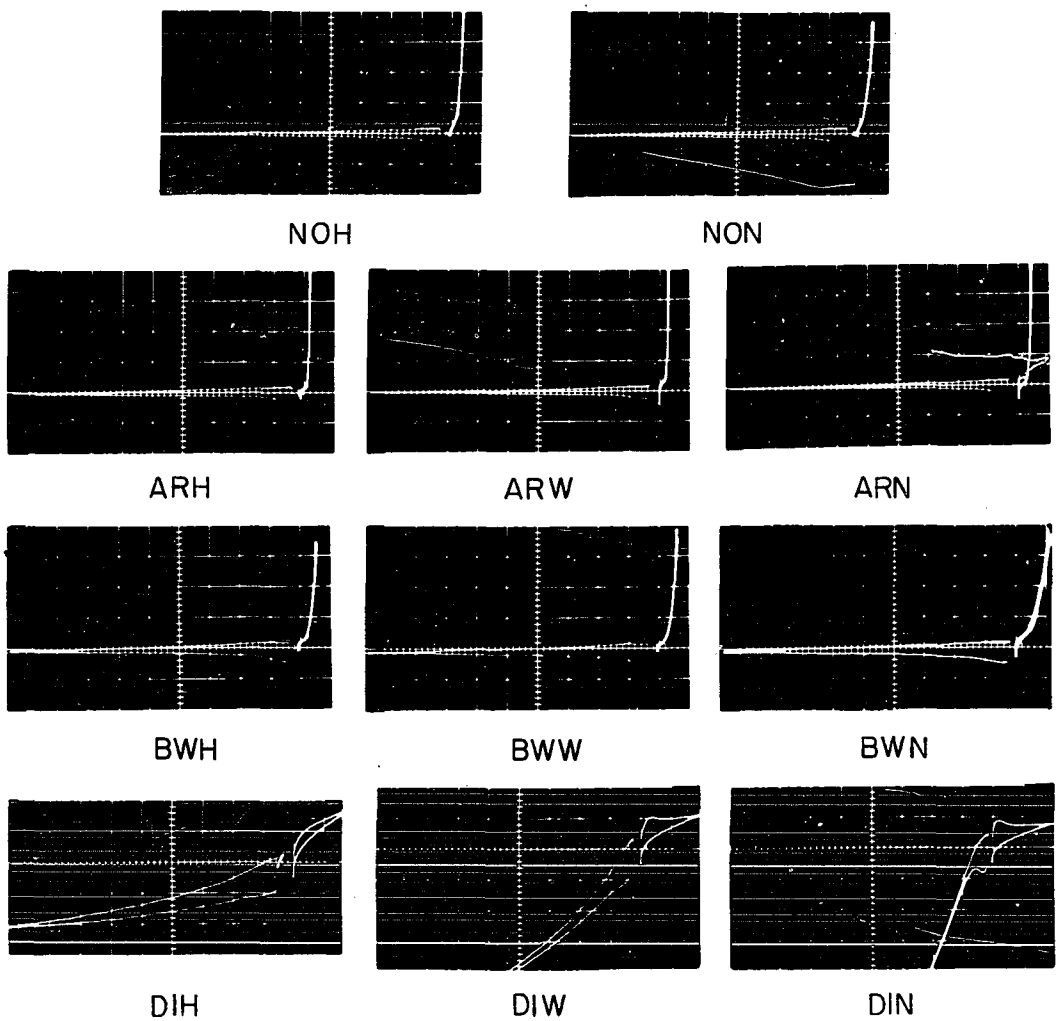

Fig. 10 Curve Tracer Characteristics of Surface Barriers After One Week of Storage In Filtered Room Air

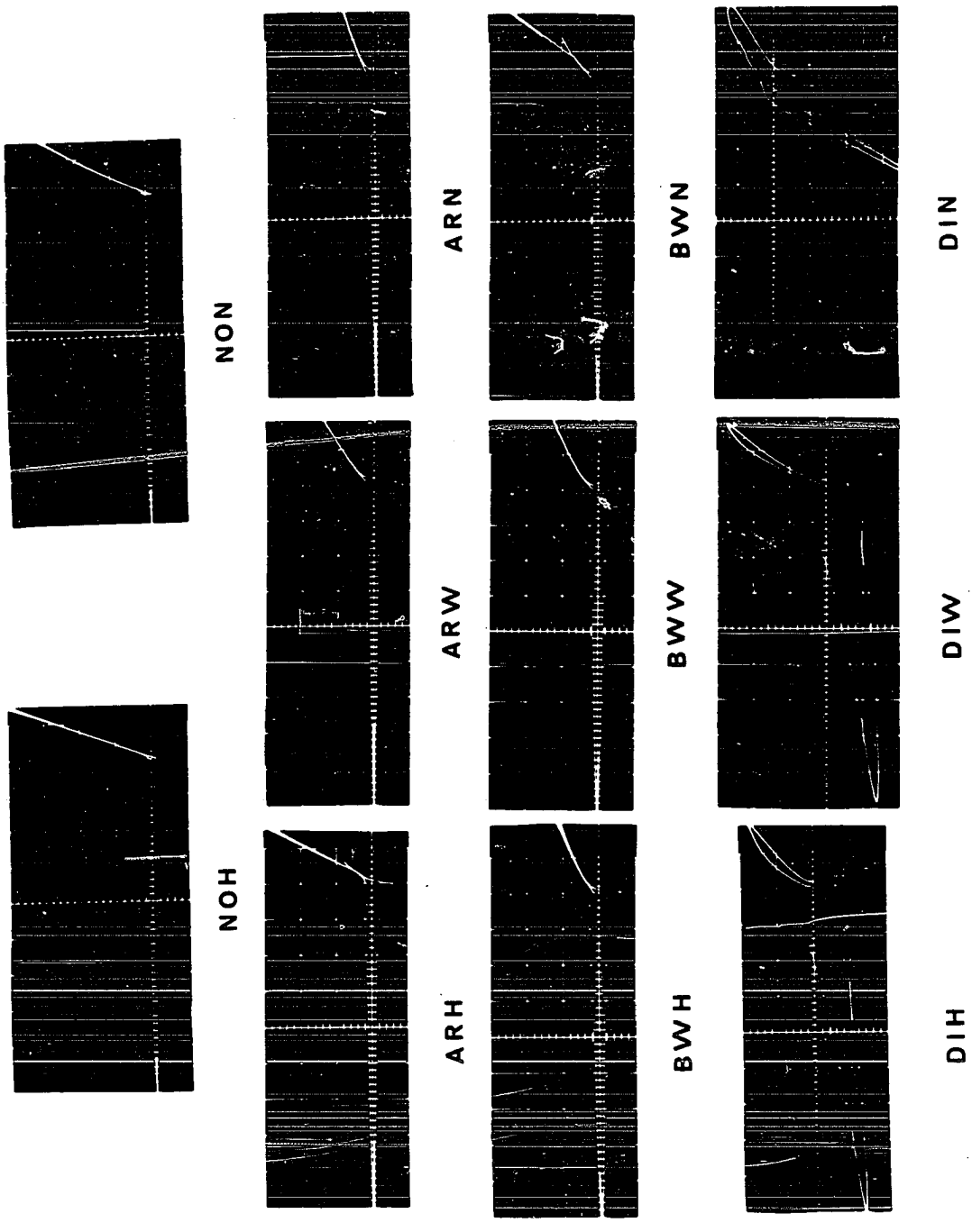

Fig. 11 Curve Tracer Characteristics of Surface Barriers After Seven Months of Storage in Filtered Room Air

characteristic curve is caused by junction and stray capacitances. For these measurements, the surface barriers were shielded from light and were mounted within six inches of the curve tracer input terminals in order to minimize stray capacitance.

After one week of storage in clean air, measurements were also made for detailed point by point current-voltage characteristics on all surface barriers except those treated with potassium dichromate. For the surface barriers of the DI group, the reverse currents were so large even at low voltages that curve tracer photographs were quite accurate for them. These point by point measurements were made using a 1500 volt regulated dc power supply, a 10 megohm current limiting resistor, a Boonton Model 95A picoammeter and the surface barrier, all connected in series. The surface barrier was mounted in a specially constructed metal chamber which was a good electrical and light shield and which could hold a high vacuum. Each surface barrier was tested at atmospheric pressure up to a reverse voltage of almost 1500 volts. Figures 12, 13 and 14 show the reverse characteristics of the NO, AR and BW groups of surface barriers respectively.

The results of the curve tracer and detailed current-voltage characteristics can be summarized as follows:

1. With respect to both forward and reverse characteristics, the surface treatments can be ranked in a decreasing order of superiority as 1) NO, 2) AR, 3) BW and 4) DI. There is some ambiguity about the ranking of AR and BW.

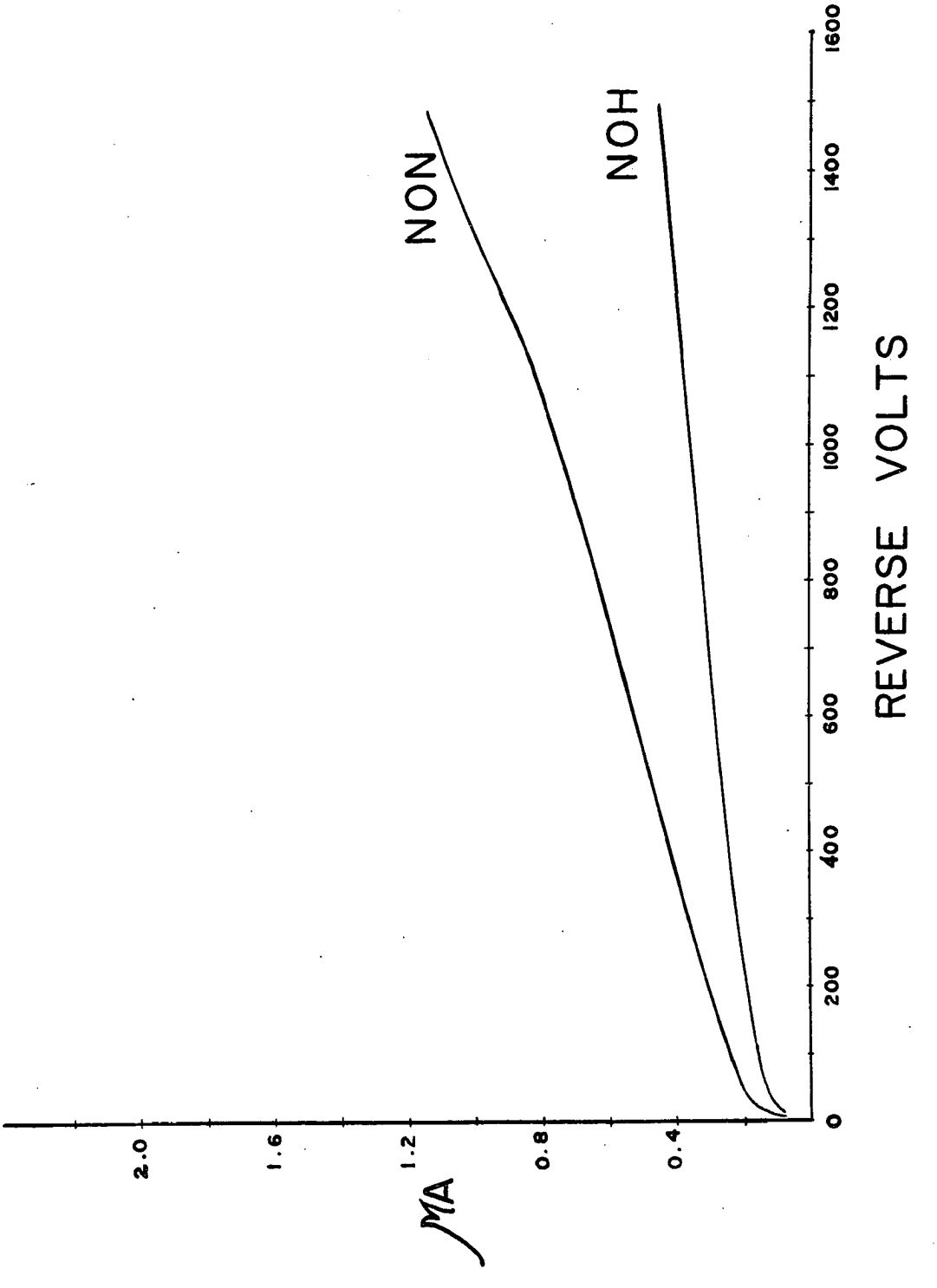

Fig. 12 Reverse Characteristics of the NO Group of Surface Barriers

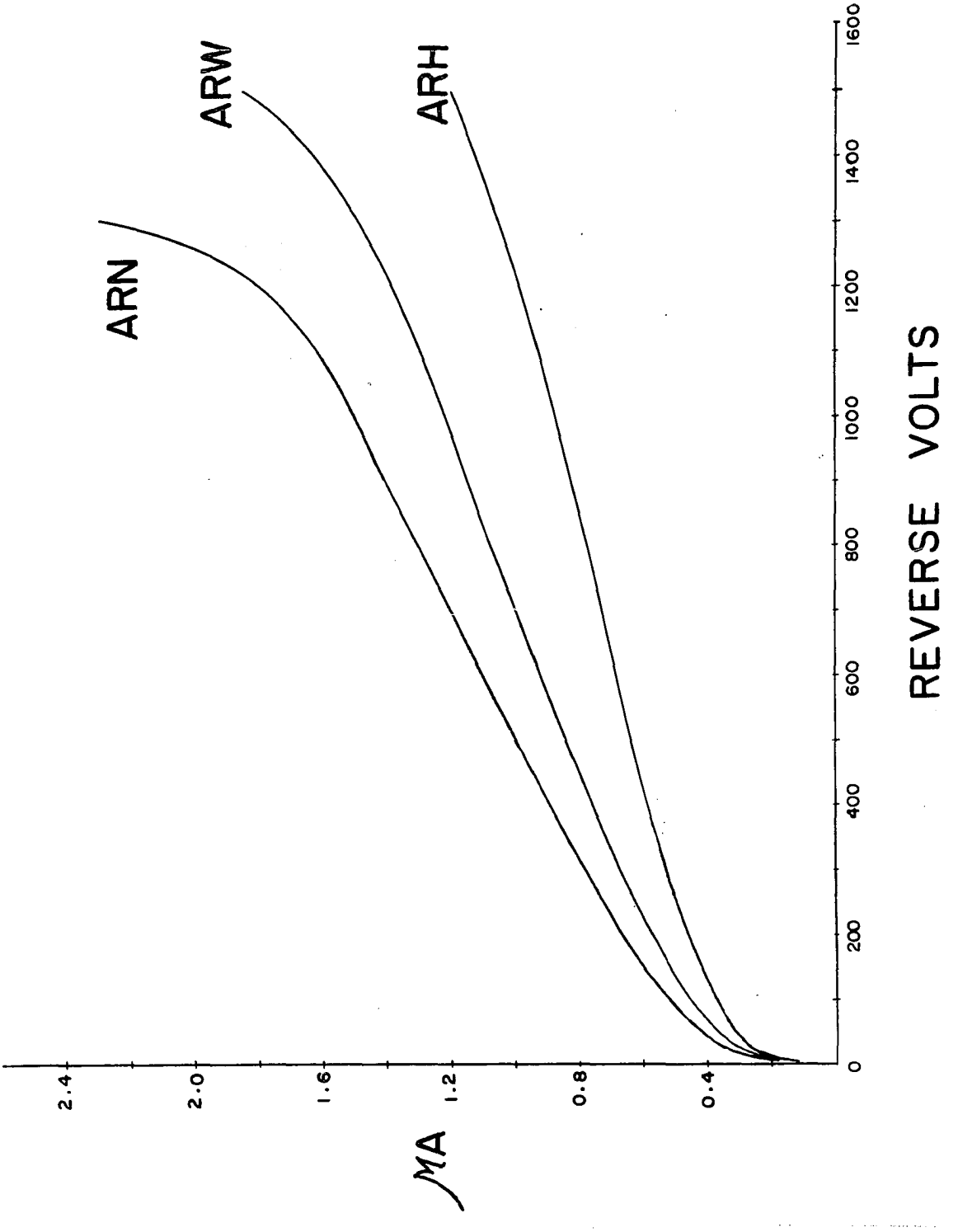

Fig. 13 Reverse Characteristics of the AR Group of Surface Barriers

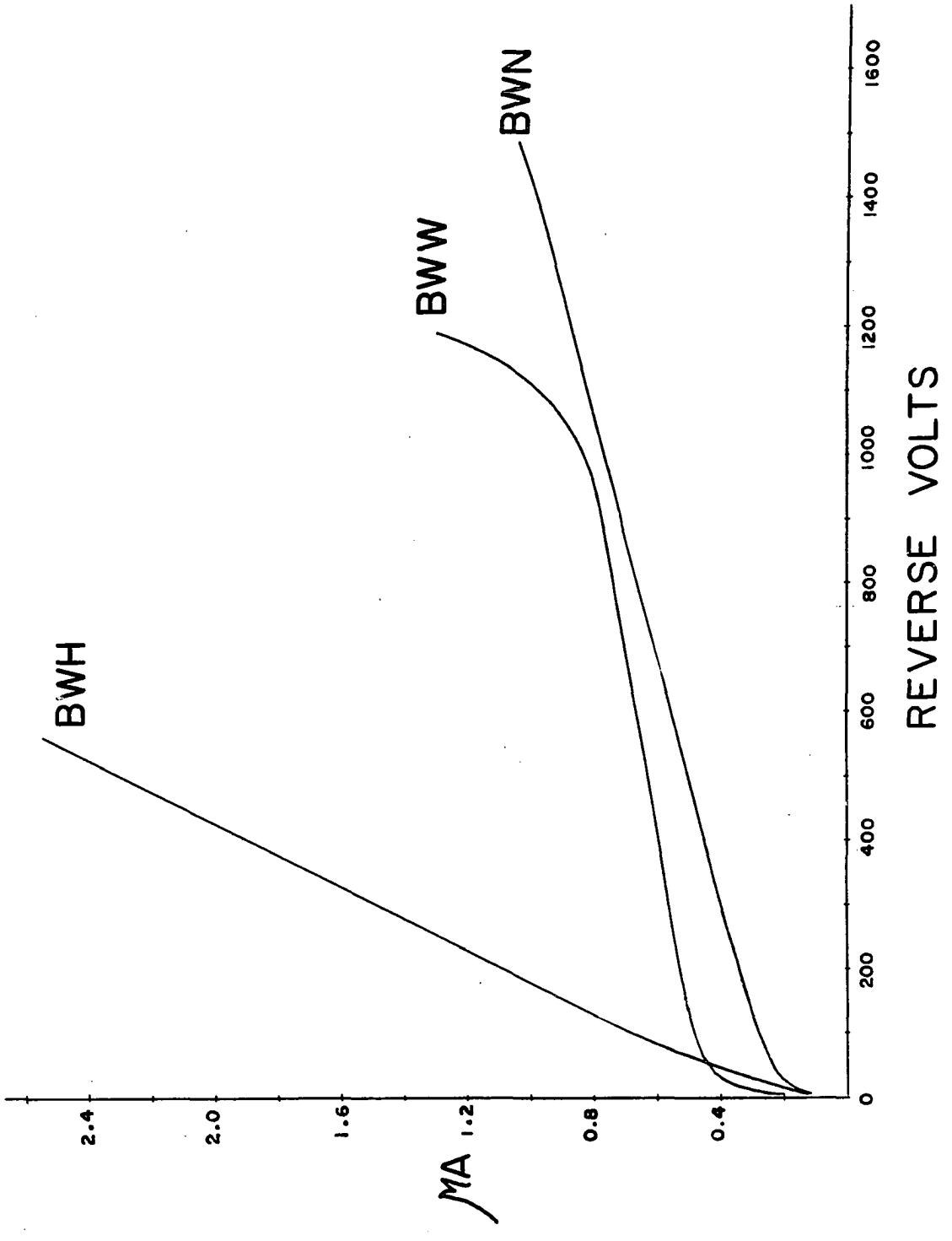

Fig. 14 Reverse Characteristics of the BW Group of Surface Barriers

2. The quenchants can be classified in a decreasing order of superiority as 1) HF 2) H_2O and 3) HNO_3 for the NO, AR and DI surface treatments and in the decreasing order of 1) HNO_3, 2) H_2O and 3) HF for the BW surface treatment.

3. The DI surface treatment does not produce good rectifiers but it appears to be extremely useful in the evaluation of the different quenchants, at least for the NO and AR surface treatments, since it clearly distinguishes among them in the curve tracer characteristics.

4. The combination of surface treatment and quenchant which gives the best reverse characteristic also gives the best forward characteristic. It must be noted that if the back contact to the silicon bulk material is not a perfectly non-rectifying contact, then it will be reverse biased when the gold-silicon contact is forward biased. Thus, the forward characteristic actually depicts the quality of the bulk contact. We can then say that the same mechanism which causes a good reverse characteristic of the Au-Si surface barrier also causes a non-rectifying bulk contact.

5. After seven months of aging in filtered room air, the bulk contact becomes more rectifying. However, the previous comments still apply in the sense that the better the Au-Si surface barrier, the slower the deterioration of the bulk contact.

6. For the BW surface treatment, the reverse current

characteristics indicate that the decreasing order of superiority for quenchants is 1) HNO_3, 2) H_2O and 3) HF. However, for the same surface barriers, the forward characteristics on the curve tracer indicated a reverse order for the quenchants after one week and the same order as given above after seven months.

Differential Capacitance Measurements for the Evaluation of the Diffusion Potential

The diffusion potential of a metal-semiconductor surface barrier is most commonly evaluated by the method of differential capacitance measurements. Under the condition that the semiconductor space charge is comprised of ionized impurity atoms only (that is, when there is no inversion layer), the ac differential capacitance of a metal-semiconductor surface barrier is given by

$$\left(\frac{C}{A}\right)^{-2} = \frac{2}{q\varepsilon_r\varepsilon_o N_D}(V_d + V_a) \qquad (62)$$

where $\frac{C}{A}$ is the capacitance per unit area, N_D the donor density for an n-type semiconductor (assumed fully ionized in the space charge region), V_d the diffusion potential and V_a the applied voltage and q, ε_r, ε_o have been defined before. Thus, if $\frac{1}{C^2}$ is plotted against the applied reverse voltage, there will be an intercept on the negative voltage axis equal to V_d.

The differential capacitance measurements were made with a Boonton Model 74C-S8 sensitive capacitance bridge with a 50 mV peak-to-peak 100 KHz internal test signal. The reverse voltage

bias could be applied with an internal dc power supply and measured with a null-type Fluke Model 887A dc differential voltmeter.

When the differential capacitance measurements were made on the surface barrier NOH, it was found that as the reverse bias was varied from one value to another, there was a slow relaxation effect in the capacitance at each reverse voltage. For example, suppose a reverse bias of 0.2 volts had been applied for a long time, say 1 hour, and the steady state capacitance had been measured. Then when the reverse voltage was changed to 0.4 volts, the capacitance would at once decrease as expected and then over a period of 20-30 minutes, it would increase by a significant amount (as much as 10% of its value at the lower voltage) and settle down at a new value for 0.4 volts. The same kind of behavior would be observed when the voltage was changed from 0.4 to 0.6. At each reverse voltage a slight change in reverse current was also observed. For example, when the voltage was changed from 0.2 to 0.4, the reverse current would at once increase, as expected, and then relax back to a slightly smaller value with time. At higher reverse voltages the relaxation became less and less until it vanished around 20 volts or so.

If the measurements were made with the reverse voltage decreasing in steps from a high value, an exactly similar but reverse relaxation of capacitance was observed. That is, at a smaller reverse voltage, the capacitance increased at first and

then relaxed to a smaller value.

NON and ARH were found to exhibit exactly similar behavior. Differential capacitance measurements were not performed on other surface barriers because the relaxation of capacitance would render the diffusion potential values unreliable. It was fully confirmed that the relaxation effects observed were truly due to the surface barriers and not the electronics. Replacing the surface barrier by a fixed capacitor of similar value showed no such effects at all. Fig. 15 shows a representative curve of the variation of capacitance with time for the surface barrier NON, with the reverse voltage increasing.

Investigation of Capacitance Relaxation Effect by Alpha Particle Probing Experiment

The following model was arrived at in order to explain the slow relaxation of the differential capacitance.

Fig. 16a shows an Au-n-Si surface barrier in equilibrium at some reverse voltage, say 2 volts. At this voltage, it will have a certain depletion width and a corresponding differential capacitance and reverse current. The space charge region in the silicon will have a slightly larger area than that of the gold electrode. Due to the edge effect, the electric field lines from the periphery of the gold electrode will terminate into the silicon space charge not directly below but a little further away. This will give rise to a tangential component of the electric field

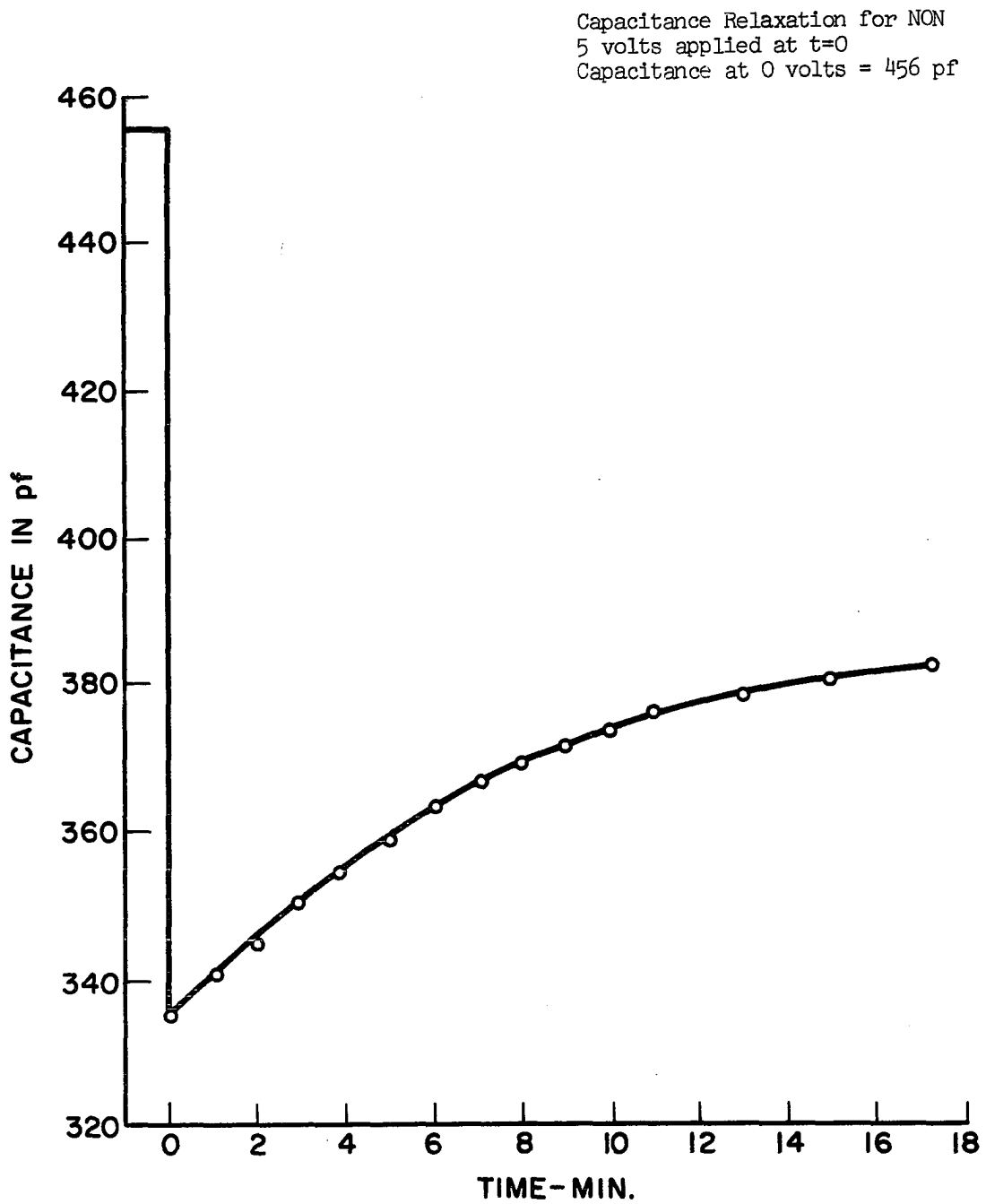

Fig. 15 Time Relaxation of Capacitance for the Surface Barrier NON

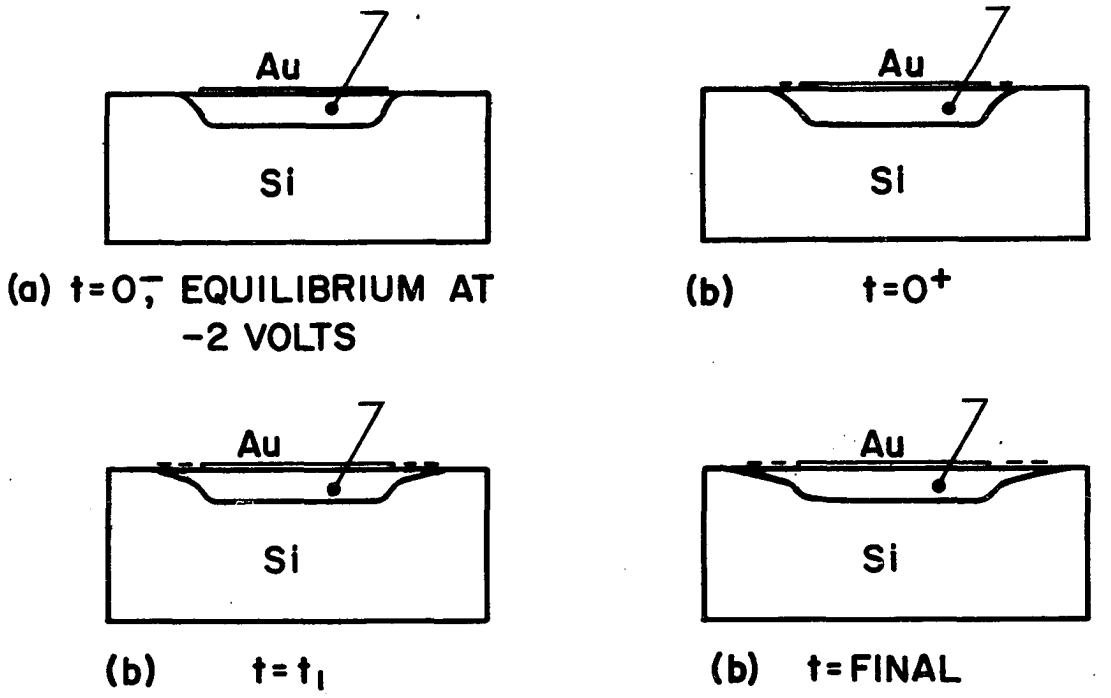

(b) Stages in the Spreading of Space Charge Due to Negative Ion Migration on the Silicon Surface

Fig. 16

Figure Illustrating the Capacitance Relaxation Model

along the silicon surface in the vicinity of the periphery of the gold electrode.

Now suppose that the reverse voltage is changed to 5 volts. This at first causes the depletion width to increase, with a corresponding decrease in the differential capacitance. The lateral spread of the space charge will also slightly increase and so will the tangential component of the electric field on the silicon surface. The tangential electric field will cause the migration of the chemisorbed ions. With a reverse voltage, the direction of the tangential field will be towards the gold electrode so that negative ions such as those of oxygen will tend to move away from the electrode. This surface migration of the chemisorbed ions must presumably be slow in order to explain the relaxation time of several minutes. As the surface ions migrate away from the gold electrode, the silicon space charge underneath will also tend to spread further, thereby increasing the differential capacitance. This is shown in Fig. 16b. Also, as the overall area of the space charge region increases, the reverse current decreases by a very small amount, presumably due to the reduction in the bulk diffusion current. The equilibrium capacitance will thus be slightly higher than its value soon after increasing the reverse voltage. When the reverse voltage has reached a sufficiently high value, the width of the depletion region will be quite large, even beyond the periphery of the gold electrode, and most of the ionic charge will already have been

migrated so that the space charge, and hence the differential capacitance will not significantly change any further.

By an exactly similar reasoning, it can be seen that when the reverse voltage is decreasing, the capacitance at each lower voltage will at first increase and then relax back to a lower value.

In order to experimentally confirm the above model, it was decided to conduct the following experiment.

Suppose a finely collimated beam of monoenergetic alpha particles is incident normally on a surface barrier a little beyond the edge of the gold electrode. If the surface barrier is used as a nuclear spectrometer in conjunction with proper amplifiers and a multichannel pulse height analyzer and if the range of the alpha particle is much larger than the depletion width at the point of incidence, then the peak of the pulse height spectrum will correspond to an energy which is proportional to the depletion width. When the reverse voltage is changed, then if the peak of the pulse height spectrum shifts with time, that must correspond to a change in depletion width with time as required by the above model. By measuring the time variation of the peak of the pulse height spectrum, as a function of both different increasing and decreasing voltages and different distances from the edge of the gold electrode, a complete mapping of the width of the space charge as a function of time, reverse voltage and distance from the gold electrode can be made.

A detailed alpha particle probing experiment as described above was not carried out but time variation measurements made at two different distances from the gold electrode edge did show a time shift of the peak of the pulse height spectrum as expected. These results are shown in Table 2. There were several experimental difficulties associated with this experiment which could not be completely overcome so that these results should be regarded as only a qualitative confirmation of the model presented above.

Table 2

Time Variation of Alpha Energy at Position 1

	Reverse Voltage 1 Volt	Reverse Voltage 2 Volts	Reverse Voltage 5.04 Volts
Time min	α MeV	α MeV	α MeV
0	1.236	2.293	3.481
1.65	1.256	2.488	3.509
3.30	1.297	2.514	3.512
4.95	1.329	2.536	3.512
6.60	1.342	2.533	3.522
8.25	1.352	2.570	3.507
9.90	1.360	2.558	3.516
11.55	1.369	2.577	3.513
13.20		2.583	3.514
14.85		2.594	3.518

CHAPTER V

FIELD EFFECT MEASUREMENTS

Introduction

The theory of the low frequency ac field effect measurements was presented in Chapter III. Although the idea of using a capacitively applied transverse electric field to modulate the conductance of a thin semiconductor filament had been used previously, Brown was the first to show in 1955 that the surface potential as well as the densities and energy positions of fast surfaces states could be evaluated from such measurements when a conductance minimum was obtained.[31]

Experimental Arrangement

In order to derive the experimental ΔG versus Σ_{in} curve ($\Sigma_{in} = \Sigma_{fss} + \Sigma_{sc}$, is the field induced surface charge density) from the measured parameters of the field effect experiment, it is necessary to describe the experimental arrangement first. This is shown schematically in Fig. 17 and is described in the following paragraphs.

A constant current, I , equal to about 1 mA is made to flow through the n-type silicon filament under investigation by

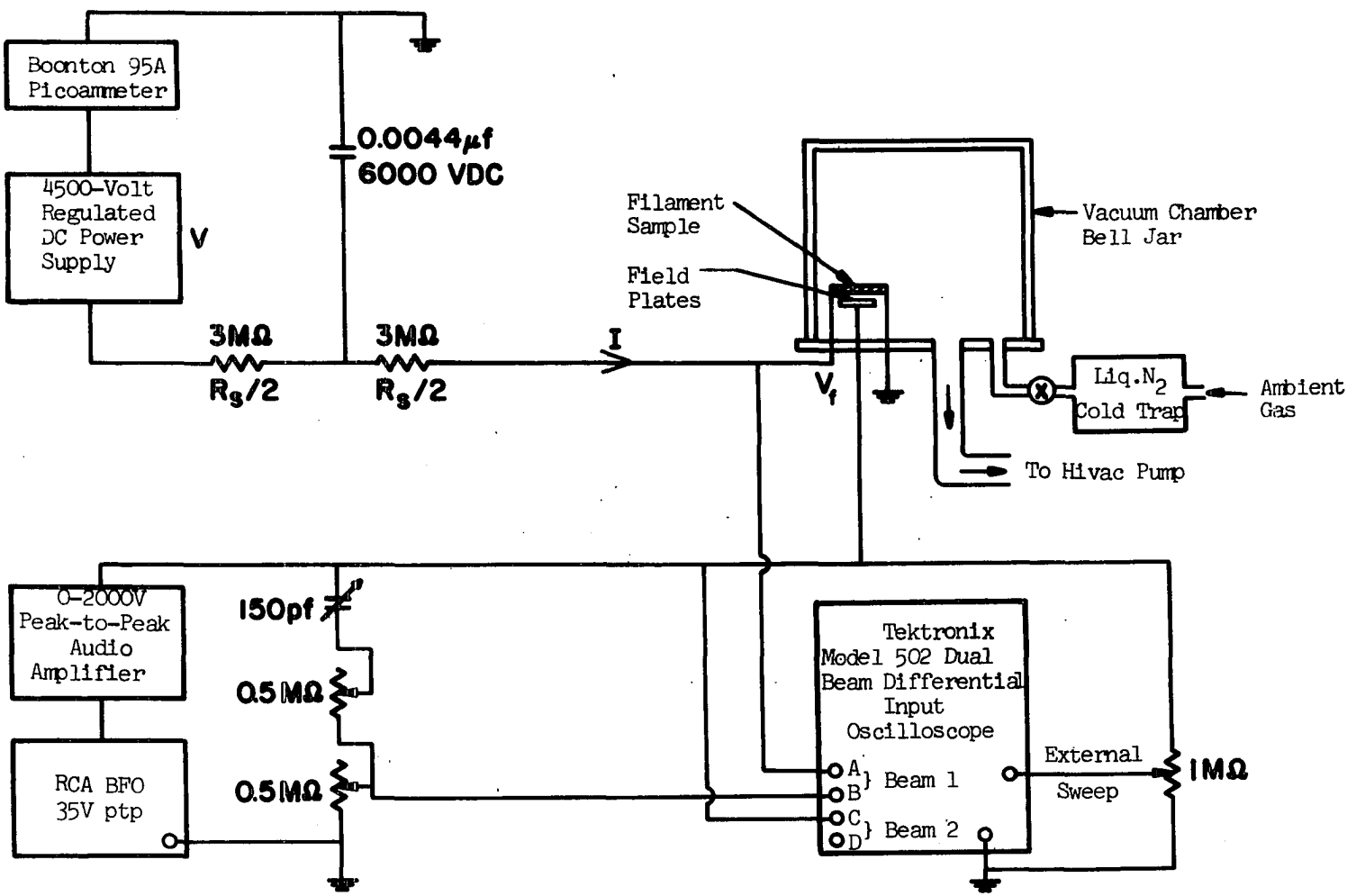

Fig. 17 Schematic Diagram of the Arrangement for the Field Effect Measurements

connecting it in series with a large resistor R_s and a high dc voltage V . The current flows along the length of the sample whose dimensions are approximately 2 cms x 2 mm x 0.2 mm and which has two non-rectifying contacts at the ends. The sample is placed within an ambient control chamber where it can be kept under a high vacuum or under any desirable gaseous or vapor ambient. A 250 Hz, 0-2000 volts peak to peak ac sinusoidal generator is connected to two metal field plates which are applied to the broad surfaces of the sample and separated from them by thin pieces of mica. Part of this ac voltage forms the horizontal sweep of a differential amplifier input dual beam oscilloscope. The ungrounded or signal end of the sample is ac coupled to input A of the upper beam input amplifier whose input B is fed by a compensating RC network whose function is to anull that part of the field effect signal which is due solely to the capacitively induced displacement current. The full ac field plate voltage is applied to input C of the lower beam, and its function is to provide monitoring of the horizontal and vertical voltage magnitudes. When both the dc and ac voltages are applied, curves such as are shown in Fig. 18 are obtained, where the upper straight line is the monitoring ac voltage and the lower curve is the conductance modulation curve.

Let R, g denote the resistance and conductance of the sample in the absence of an ac field. Then g is actually the parallel conductance of the central core where the bulk free carrier densities prevail and the two surface space-charge regions

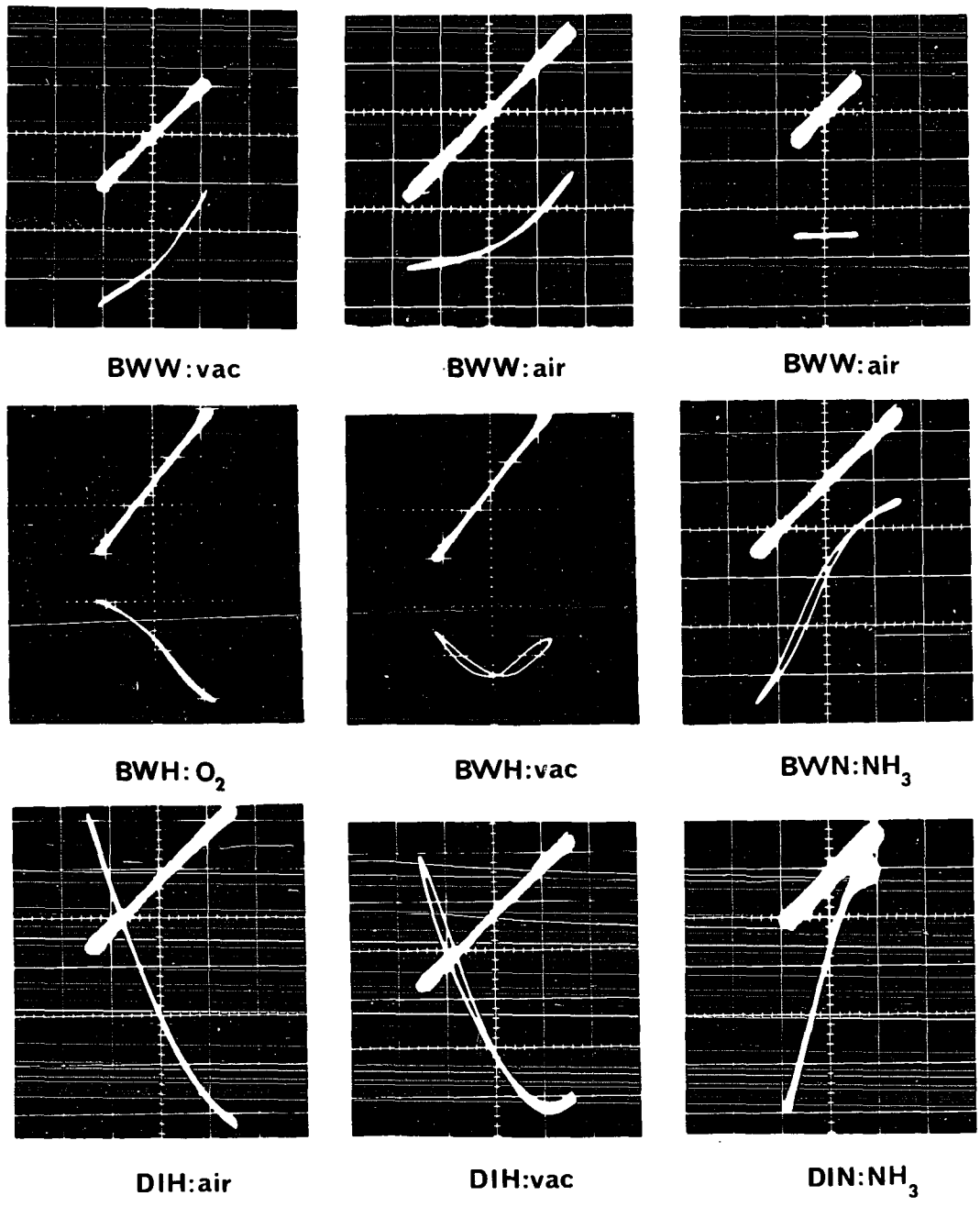

Fig. 18 Representative Oscilloscope FE Curves for the BW and DI Groups of Surface Treatments

of the broad faces. With a constant current I flowing through the sample, the dc voltage across the filament will be $V_f = IR = \frac{I}{g}$. Now when the ac voltage is applied to the field plates, an alternating electric field will be set-up in the region between each field-plate and the corresponding surface of the sample.

Let $v_{ac} = V_o \sin \omega t$ be the field plate voltage. Then the charge density induced on the silicon surface is

$$\Delta\Sigma_{in} = \frac{Cv_{ac}}{2A} \tag{63}$$

where C is the low frequency capacitance between the field plates and the sample, and A is the effective area of the sample surface under each field plate.

The induced space charge density will change the conductance of the space charge region according to the relation expressed by the theoretical ΔG versus Σ_{sc} curve. Thus the filament conductance will be changed by an amount Δg and if the current is maintained constant, a voltage ΔV_f given by

$$\Delta g = - \frac{I}{V_f^2} \Delta V_f \tag{64}$$

will appear at the input A . Since $V_f = IR$,

$$\Delta g = - \frac{\Delta V_f}{IR^2} \quad . \tag{65}$$

Now, in order to convert Δg into conductance per square we must have

$$\Delta G' = \frac{\ell}{2w} \Delta g = - \frac{\ell}{2w} \times \frac{\Delta V_f}{IR^2} \quad . \tag{66}$$

Here ℓ and w are the effective length and width of the filament sample actually under the field plate, I the constant current through it, R its resistance under the particular ambient under zero ac field and ΔV_f the observed voltage variation. Here, $\Delta G'$ does not represent the surface conductance with respect to flatband conditions but rather with respect to the field-free surface potential under the given ambient. It is only when the conductance minima of the experimental and theoretical curves are aligned that the true values of ΔG with respect to flatbands can be obtained for each point of the experimental curve. Using equations (66) and (63) we can transform the observed field effect curve on the oscilloscope into an experimental $\Delta G'$ versus Σ_{in} curve.

As pointed out earlier, in practice it is hardly ever possible to obtain a single experimental field effect curve under any given ambient which will cover a wide range of $\Delta G'$ versus Σ_{in} variation and will include the conductance minimum. Electric fields as high as 10^5 volts/cm fail to produce a wide enough swing of the surface potential so that what is obtained in practice is a small field-induced swing in surface potential around each of its

quiescent values as determined by the ambient. One thus has to subject the sample to an ambient cycle which successively swings the surface potential from that corresponding to an accumulation region to that for an inversion region. The fragmentary curves for the different ambients are then superposed where they overlap to form a smooth continuous curve of ΔG versus Σ_{in}. Even so, it is quite often not possible to obtain a conductance minimum, especially in the case of silicon which has a relatively wide forbidden band. The fact that it is possible to fit the different fragments into a single curve is a direct indication of the fact that it is only the fast surface state densities which change with ambient and not their energy positions in the forbidden band.

Preparation of the Silicon Samples

The silicon samples used in the field effect measurements were in the form of filaments of average dimensions 1.7 cm x 3.2 mm x 0.25 mm. This form is best suited for field effect measurements since it affords the large surface to volume ratio necessary to resolve the small field induced conductance modulation from the large shunting bulk conductance. Several 0.5 mm thick slices were cut with a thin blade diamond saw from a cylindrical ingot of 450 ohm-cm n-type silicon with the cylindrical axis being perpendicular to the (111) faces. These slices were lapped with American Optical M302 and M303 abrasives on a ground glass plate until the faces showed no mechanical damage due to sawing. The

lapped slices were then cut into filaments with the help of a diamond scribe. The filaments were again lapped until their thickness was around 0.3 mm. The filaments were then cleaned in an ultrasonic detergent bath, rinsed thoroughly in deionized water, subsequently cleaned in ultrasonic TCE bath and dried on filter paper. These were then stored in petri dishes in a dust-free enclosure. After the final lapping of the filaments, they were untouched by hands and were handled only with polyethylene or teflon coated tweezers which were rinsed thoroughly in deionized water each time before use.

For each field effect run, two samples were etched and surface treated simultaneously to insure against one of them not being suitable for measurements. The filaments were etched in 100 cc of CP4-A etch for 4 minutes while being stirred vigorously and holding the etching beaker in ice-cold water. The etch mixture was freshly prepared for each run and was cooled for 2-4 hours in ice before being used. After exactly 4 min. of etching, the filaments were quenched with either HF, deionized water or HNO_3 as described before.

About 10 to 15 seconds after adding the quenching agent, the etching mixture was diluted with slowly running deionized water until the resistivity of the overflowing water was at least about 3 megohm-cm. The filaments were thus thoroughly rinsed to ensure the absence of any residual acids on their surfaces. The samples were then given the same set of surface treatments as the surface

barriers, which were described earlier.

Extreme care was taken to prevent exposure to air during the entire process of etching, rinsing and surface treatment. Even after the surface treatment, a maximum of 10 min. of exposure to air was allowed. During this time, the filaments were dried on filter paper, gently scratched on both sides at each end with a diamond scribe and then masked off with mica pieces and placed in the high vacuum evaporator for deposition of aluminum contacts over the ends. The evaporator system was so set-up that aluminum could be simultaneously evaporated on both sides so as to again eliminate exposure to air during changing of face. A film thickness in excess of 1000Å of Al was evaporated under a high vacuum of below 5×10^{-5} mm. of Hg. At least 2 hours of pumping was used to insure as little thickness as possible of the interfacial layer between Al and Si.

One of the filaments was then removed from the high vacuum and stainless steel foil field plates with clean cleaved mica spacers were quickly attached to it. The field plates were held by alligator clips. This kind of a mounting arrangement was chosen after trying several others because it provides a minimum of air gap between the field plate-mica-silicon capacitor. After etching, the crosssectional shape of the filament becomes sometimes like that of a convex lens, thus requiring flexible field plates for maximum coverage. After mounting the field plates, two single-strand wire leads about 3 inches long were attached at each end over the

evaporated aluminum with Anchor Alloy silver paste. The silver paste has a tendency to cause a strong inversion layer under it so that care was taken to not let the silver paste touch the silicon beyond the evaporated aluminum. The fairly thick film of Al also helped in preventing the silver paste from penetrating it and reaching the silicon. The leads were attached after mounting the sample within the ambient control system, so that it could be quickly placed under a high vacuum without having to wait for the silver paste to dry in air. Thus the sample was exposed to air for only about 20 min. between the time it was removed from high vacuum after Al evaporation and the time it was again in high vacuum ready for field effect measurements.

The need for non-rectifying contacts for the success of field effect measurements cannot be overemphasized. Excessive variation of contact resistance with ambient renders the field effect measurements useless for any quantitiative information; first by introducing errors that cannot be corrected and secondly by preventing the attainment of the conductance minimum. Considerable effort was spent over a period of almost two years to achieve non-rectifying contacts onto high resistivity silicon. This effort met with only partial success. Contacts made on evaporated Al over scratched surfaces were generally found to be good provided exposure to air prior to Al evaporation was minimized. Even so, the contacts remained good in air for only a few days or weeks. This may explain why two filaments were prepared simultaneously and

why exposure to air was minimized.

Field Effect Measurements

The experimental arrangement was as described earlier and as shown in Fig. 17. The dc voltage was obtained from two high voltage regulated power supplies stacked in series to give about 4500 volts. The series resistance was 6 megohms which gave a dc current of about 740 microamperes through the sample. A Boonton Model 95A Sensitive DC Meter was used to read and monitor the dc current. The filament resistances were of the order of 100 kilohms and varied by as much as ± 30 kilohms under different ambients but much less over the entire swing of the ac field. Thus the dc current was substantially constant. The correction for not having an ideal current source for I is given by

$$\Delta V_{f(true)} = \Delta V_{f(observed)} \times \left(1 + \frac{R}{R_s}\right)^2 , \qquad (67)$$

where R is the dc filament resistance under a particular ambient and the other quantities have been defined previously. With R = 100 kilohm and R_s = 6 megohm, the correction is seen to be less than 3 per cent. Proper corrections were applied to all the experimental ΔG versus Σ_{in} curves. It may be pointed out that use of a larger series resistance would have made the correction negligible but it would have either made it necessary to use an unduly high dc voltage with its associated breakdown problems or it

would have reduced the dc current with a subsequent reduction in the resolution of the measurements. Of course, the dc current must be limited to a safe level that does not heat the filament since under a vacuum ambient, the heat losses through the leads may be insufficient.

The frequency of the dc field was 250 Hz. The ac frequency is not critical and no detectable change in the field effect measurements was observed over a wide range of frequencies of from 40 Hz to about 1 kHz. The frequency must be within this range because it must be high enough to eliminate effects of slow states and low enough to include all fast states, that is, to maintain an equilibrium between all the fast states and the energy bands. The ac voltage was obtained from an audio oscillator and a high voltage audio amplifier which was capable of giving a sinusoidal voltage of 2000 volts peak-to-peak. Most of the time, however, a field plate voltage of only 800 volts peak-to-peak was used.

The compensating network was made up of an air dielectric 150 pf variable condenser in series with two 0.5 megohm potentiometers, the output being at the connection between the two potentiometers. When an ac voltage is applied to the field plate, the output voltage across the filament consists of two components: 1) a voltage which is almost 90° out of phase with the applied ac voltage and is due to the charging of the field plate-silicon capacitor through the relatively small filament resistance, and 2) a voltage which is in phase with the applied ac voltage and due

to the modulation of surface conductance. The purpose of the compensating network is to cancel the out of phase displacement component. With zero dc current flowing through the filament, the compensating network is adjusted to give a horizontal straight line on the scope indicating that in the absence of any conductance modulation signal, the cancellation of the out of phase signal is perfect. This condition is not always easy to achieve, especially when a particular ambient causes an inversion layer, thus leading to high contact resistances at the two ends of the sample. If this condition is achieved, then only a slight adjustment should be necessary to get a good field effect curve when the filament dc current is not zero. Quite often the conductance modulation signal is so large compared to the displacement signal that compensation becomes a simple matter.

The field effect curves were obtained directly on the Tektronix Model 502 differential amplifier input dual beam oscilloscope with a Polaroid camera attachment. The scope was calibrated with the help of the audio generator and a Fluke Model 887A AC/DC differential voltmeter. The horizontal sweep for the scope was obtained from the field plate voltage through a potential divider.

For each ambient, the dc current was noted. A calibration curve was made to obtain the dc filament resistance from the dc current. The ac voltage was then gradually increased from zero up to about 800 to 1000 volts peak-to-peak. Under some ambients, only

a small ac voltage was possible due to voltage breakdown. The resulting field effect curve was photographed for each ambient. In practice, a time record was kept and photographs were taken at certain time intervals during an ambient cycle.

The Ambient Cycle

A definite ambient cycle was evolved after trying a large number of different ones. Field Effect Curve photographs were taken at approximately the following times during the ambient cycle which is described below.

1. In air soon after mounting and attaching leads.
2. In vacuum at about 2×10^{-4} torr after 1 hr. of diffusion pumping.
3. In vacuum at 5×10^{-5} torr or less after at least 12 hours of diffusion pumping.
4. Within the first minute after letting in dry oxygen for 30 seconds. The oxygen was obtained from a Linde high pressure oxygen cylinder through a liquid nitrogen cold trap to condense any moisture in it. Oxygen was let into the bell jar at a slow rate for 30 seconds after which the bell jar was sealed off.
5. 3 min. after letting in oxygen.
6. Anywhere between 6 and 10 min. after letting in O_2.
7. Within one minute after letting in dry SO_2 for 15 seconds. The SO_2 was freshly prepared by reacting $NaHSO_3$ (sodium

sulphite) with concentrated sulphuric acid, in a glass flask which was connected to the liquid N_2 cold trap. With the O_2 still within the bell jar at below atmospheric pressure, the SO_2 was sucked in along with room air just by opening slightly the bell jar vent valve.

8. About 3 min. after letting in SO_2.

9. About 6 to 10 min. after letting in SO_2.

10. Within one minute after letting in dry N_2O for 15 secs. N_2O was obtained by heating NH_4NO_3 crystals in a flask and was sucked in through the cold trap, along with room air, in the presence of O_2 and SO_2.

11. About 3 min. after N_2O intake.

12. About 6-10 min. after N_2O intake.

13. In vacuum after pumping for anywhere between 15 min. and a few hrs.

14. In moist air obtained by bubbling room air through water. The moist air was let in for 15 secs. or sometimes even for a few minutes.

15. In moist NH_3 obtained by bubbling room air through an aqueous solution of NH_4OH. The NH_3 was let in for 15 to 30 seconds.

16. In vacuum after pumping out NH_3. Sometimes, several photos were taken during prolonged evacuation.

17. In room air, soon after letting in air following evacuation of NH_3.

18. After 30 min. or so in room air.

The ambient cycle described above is only meant to give an outline of the ambients used and the relative time intervals at which the field effect curve photographs were taken. Neither the ambients not the times were rigidly followed for each sample since the primary purpose of the ambient cycle was to help obtain a conductance minimum so as to be able to evaluate the surface potentials in room air, moist air and vacuum. Thus the ambient cycles and times of photographs differed slightly from sample to sample and were always chosen to yield the best possible set of partially overlapping field effect curves. A representative set of field effect photographs is shown in Fig. 18.

Results of the Field Effect Measurements

The oscilloscope photographs of the FE (field effect) curves represented ΔV_f versus v_{ac}, which could then be converted into $\Delta G'$ versus $\Delta \Sigma_{in}$ by use of equations 66 and 63. In practice, all the FE curves for a given filament were first normalized to some fixed filament resistance. These were then fitted to form a single FE curve. In some cases, a conductance minimum was never obtained but could be estimated quite well by slight extrapolation of the FE curve. The position of the conductance minimum was chosen as a reference for measuring ΔV_f and v_{ac}. The field plate-silicon capacitance and the physical dimensions were measured for each filament and the experimental ΔG versus Σ_{in} curves were constructed.

Figures 19 and 20 show the experimental ΔG versus Σ_{in} curves for the NO and AR surface treatment groups. The theoretical ΔG versus Σ_{sc} curve is also present in each figure. The field-free position for some ambients are marked and the horizontal reference for each curve is arbitrarily taken as the field-free position under high vacuum after prolonged evacuation. The contact resistances for the BW and DI groups of surface treatments were very large and varied too much with the different ambients and under the ac field. Therefore, the surface potential could not be quantitatively evaluated as a function of ambients and quenchants for the BW and DI groups of surface treatments. However, useful qualitative inferences can be drawn from their FE curves. Representative FE curves for the BW and DI surface treatments are given in Figure 18.

Table 3 gives the surface potential V_s in millivolts and Σ_{fss}, the surface density of ionized fast states in units of 10^{10} cm^{-2} for the NO and AR groups. A negative surface potential means a depletion or an inversion region and a positive V_s corresponds to an accumulation region. A positive value of Σ_{fss} denotes a net positive charge stored in the fast surface states with respect to that stored under a high vacuum. Thus, the sign of Σ_{fss} has only a relative significance.

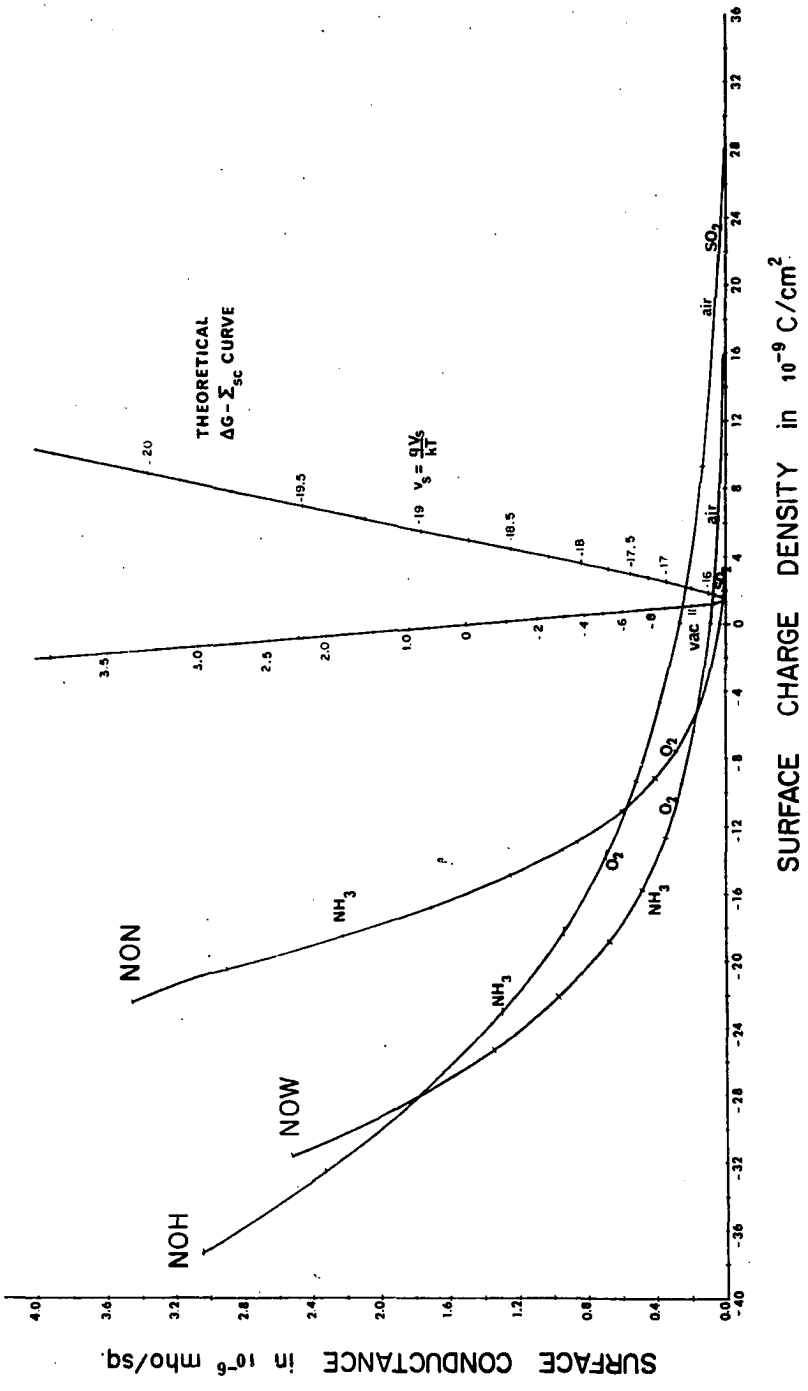

Fig. 19 Experimental ΔG vs. Σ_{in} Curve for the NO Surface Treatment

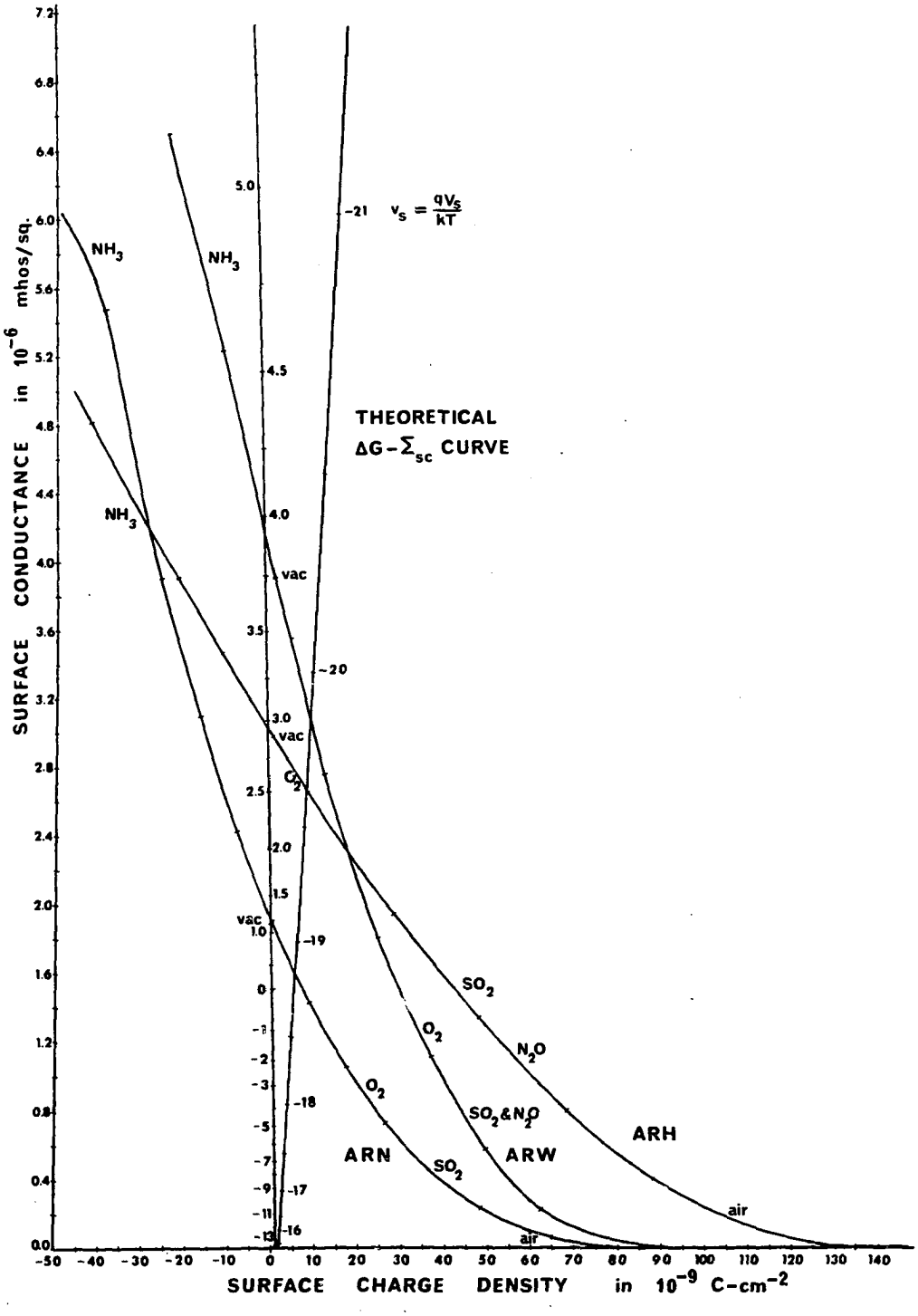

Fig. 20 Experimental ΔG vs. Σ_{in} Curve for the AR Surface Treatment

TABLE 3

Results of FE Measurements

Ambient	Surface Potential V_s in mV (Density of Ionized Fast States in 10^{10} States/cm^2)					
	NOH	NOW	NON	ARH	ARW	ARN
1. Prolonged Vacuum	-260 (-0.62)	-326 (-0.74)	-351 (-0.79)	74 (0.76)	96 (1.20)	26 (0.16)
2. ∿10 min O_2	-223 (-4.28)	-235 (-8.20)	-229 (-6.0)	67 (4.35)	-31 (21.79)	-79 (12.35)
3. ∿5 min SO_2	-329 (7.29)	-326 (-0.73)	-369 (0.31)	0 (26.2)	-116 (27.7)	-197 (22.2)
4. 2 hr. vac. after O_2+ SO_2				-104 (42.0)	-194 (32.5)	-191 (6.37)
5. 10 min vac. after O_2+ SO_2	-309 (5.29)	- -	-382 (2.58)			
6. 1.5 min NH_3	-68 (-12.7)	-265 (-6.15)	42 (-11.0)	78 (-1.25)	135 (-16.44)	124 (-25.29)
7. >10 min vac. after NH_3	-316 (6.2)	-308 (-2.68)	-311 (-2.44)	112 (-25.8)	119 (-6.87)	-19 (6.37)
8. >15 min air after ambient cycle	-313 (5.87)	-331 (2.37)	- -	-275 (67.7)	-30 (21.8)	-348 (35.9)

CHAPTER VI

DISCUSSION

This chapter includes a discussion of the results obtained. The inferences which can be drawn from the results of the current-voltage measurements and field effect measurements will be presented first. A model of the Au-n-Si surface barrier will then be given which explains many of the experimentally observed effects. Comparison will be made to the results obtained by others. Finally, some overall conclusions will be presented regarding the relative success of this research in fulfilling the motivations behind it and regarding further research that needs to be done in this area.

Inferences from the Current Voltage Characteristics and Field Effect Measurements

The following inferences can be drawn from the results of the reverse current-voltage characteristics and the FE measurements.

1. The NO, AR and BW (except for BWH) surface treatments prevent the formation of an inversion region at the silicon surface even under strong electronegative ambients. The DI surface treatment forms a strong inversion region at the Si surface. If

these FE results are correlated with the reverse characteristics, then a perfect correlation is obtained since all surface barriers except BWH and those of the DI group had low reverse currents. Also one must conclude from this that low reverse currents will not be obtained in surface barriers which have a fairly strong inversion region at the free silicon surface beyond the gold electrode. It seems that in cases where a strong inversion region appears at the free surface, either the condition $|V_d| > |V_s|$ is not realized or if it is realized, the difference $|V_d| - |V_s|$ is very small and the breakdown voltage of the B_{sc}- F_{sc} junction is small because of the large hole concentrations in each space charge region. Thus, for strongly inverted surface barriers like those of the DI group, the condition $|V_d| = |V_s|$ presumably holds and therefore large surface channel currents can flow.

2. For the NO and AR surface treatments, the quenchants HNO_3, H_2O and HF cause an increasing density of fast surface states in that order. This is indicated from the slopes of the FE curves at any v_s or ΔG . Actually, it is the quantity $d\Sigma_{fss}/dv_s$, which is the reciprocal slope of the v_s versus Σ_{fss} curve, which indicates the effectiveness of the fast surface states in shielding the space charge from an external field. This quantity is more important than just the density of fast surface states (relative to the density under some standard ambient). This is because it also takes account of the energy positions of the fast surface states and gives their overall shielding effectiveness. However, since

for most ambients, $\Sigma_{fss} \tilde{\sim} \Sigma_{in}$,

$$\frac{d\Sigma_{fss}}{dv_s} \tilde{\sim} \frac{d\Sigma_{in}}{dv_s} = \frac{d\Sigma_{in}}{d\Delta G} \times \frac{d\Delta G}{dv_s} \qquad (68)$$

and since $\frac{d\Delta G}{dv_s}$ at a given ΔG or v_s is the same for all surface treatments and quenchants, it is good enough to use the reciprocal slope $\frac{d\Sigma_{in}}{d\Delta G}$ of the experimental FE curves for purposes of comparison of the different surface treatments and quenchants. The smaller in the slope (in absolute magnitude) of the experimental FE curve at any given v_s , the less sensitive will the surface potential be to variations in chemisorbed impurities.

For the NO and AR surface treatments, the increasing density of fast surface states with HNO_3, H_2O and HF (except for ARW) can be explained on the basis of an increasing interfacial film thickness caused by these quenchants in that order. This is in accordance with Archer's results.[21] Archer found the stain films to be composed of either elemental silicon or silicon hydride so that the film is quite possibly a restructured part of the silicon surface rather than an external film and is therefore likely to contain a large number of trapping centers within it. If, therefore, it is assumed that the fast surface states reside within this film rather than at the interface between this film and the silicon, then the larger the film thickness, the larger will be the surface density of fast states. The above experimental results can then be very well explained. The anomalous behavior of the BW group cannot

be explained without reliable FE data on them.

A correlation is also found to exist between the density of fast states and the reverse current. Thus, the decreasing reverse current for HNO_3, H_2O and HF can be correlated with the increasing density of fast surface states in that order. In terms of the relative magnitudes of V_d and V_s, this result can be explained by the fact that for a given surface treatment, the larger the density of fast states, the more it will prevent B_{sc} and F_{sc} from strongly inverting.

3. It is seen from the experimental FE curves that the NO surface treatment gives rise to a smaller density of fast surface states than does the AR treatment. This result at first appears to be completely at variance with the above discussion on quenchants, since the NO group of surface barriers have a lower reverse current than the AR group. However, there is no contradiction involved if we realize that shielding by a large density of fast states is just one way of preventing F_{sc} and B_{sc} from strongly inverting. This is the mode of operation of the quenchants. The surface treatments, one the other hand, operate in an entirely different manner. It was pointed out earlier that the surface treatments influence the structure and chemical reactivity of the silicon surface. Thus, the surface treatment actually controls the amount of chemisorption of the ambient atoms or molecules by controlling their sticking coefficients. For example, if the silicon surface is in a pure oxygen ambient, then the type of surface treatment will control the

number of oxygen atoms that are chemisorbed whereas the quenchant (based on fast state densities) will control the fraction of the charge induced by the ionized O^- atoms which goes into the space charge. This means that the NO surface treatment reduces the sticking coefficients for most ambients compared to the AR surface treatment. This statement is also confirmed by the fact that for the NO surface treatment, the surface potential values are confined to a relatively narrow range (almost completely within the depletion region range) over the entire ambient cycle.

4. Under a prolonged exposure to vacuum, the AR group and BWH have a slight accumulation layer whereas the space charge for the NO group and for BWN and BWW is highly depleted and the surface potential is close to its value near the conductance minimum. This result can be explained on the basis of a large number of water molecules chemisorbed on the AR treated surfaces. Jäntsch[32] has shown that chemisorbed water can cause both slow and fast donor-like surface states. This can then explain the large density of fast states on AR treated surfaces.

5. The variations in the surface potential are not completely reversible under different ambients. For the NO and AR surface treatments, there is a tendency for the surface potential to somewhat stabilize at some final value close to that near the conductance minimum. In fact, it can be seen from Table 3 that in many cases, the surface potential is much larger in magnitude under room air after less than 30 min. of exposure after the ambient cycle

than it is under strong electronegative ambients such as O_2 and SO_2. This indicates that initially, the silicon surfaces, especially of the AR group, are predominantly covered with water molecules, a good proportion of which are gradually displaced by electronegative atoms such as O^-, as shown by Maxwell and Green[33] for Ge surfaces. Once this displacement process is complete, a somewhat stable surface potential is reached which does not change much with further ambient changes. Evidently, the displacement process takes place much faster in the NO group and BWN, BWW than in the AR group and BWH.

6. An exposure to vacuum after O_2 and SO_2 increases the magnitude of the surface potential in most cases. This indicates the loosening of the bond strengths of the water molecules by O_2 and SO_2 so that the vacuum pulls away the water molecules leaving a large number of net acceptor-like surface states. This can explain the very large degradation of surface barriers under the first vacuum exposure.

Model for the Au-n-Si Surface Barrier in the Presence of Surface States

It was shown in Chapter 3 how the relative magnitudes of V_d and V_s affect the reverse current in a gold-n-silicon surface barrier. The previous discussion, based on the experimental results, shows how the surface treatments, quenchants and ambients control the rectification characteristics of the Au-n-Si surface barrier by different mechanisms. Based on these experimental

results and those obtained by others, the following simple model is presented for the behavior of an Au-n-Si surface barrier.

After etching, the quenchant controls the thickness of the stain film which, in turn, controls the density of fast surface states. The larger the thickness of the interfacial film, the larger the number of fast states per unit surface area. It must be noted that what is observed experimentally is only the density of ionized fast states and not their total density. Thus, in order for the previous statement to be correct, the energy positions of the fast states must be essentially the same under the different quenchants. This is justified by the excellent correlation between the densities of ionized fast states and the film thicknesses.

The occupation densities of the fast states are controlled by the amount of bending of the energy bands which, in turn, is controlled by the surface treatments and ambients. The surface treatment controls the sticking coefficients of the different ambients. The sticking coefficient for a given gas or vapor molecule (or atom) is defined as the probability of that molecule (or atom) to be chemisorbed upon impinging on the silicon surface. Alternatively, the sticking coefficient is the ratio of the number of molecules or atoms that are chemisorbed to the total number impinging. The sticking coefficient will be a strong function of the coverage, that is, of the number already chemisorbed. Under a given ambient condition, the density of slow states will thus strongly depend on the surface treatment.

The prevention of a strong inversion region at the surface can be achieved by one of three mechanisms, viz.: 1) by reducing the chemisorption of acceptor-like impurities such as oxygen, or 2) by counteracting the adsorption of oxygen by an equally high adsorption of water or (3) by shielding the space-charge region with a large density of fast states. The experimental results indicate that the quenchants operate (HF operates most effectively) via the third mechanism whereas the surface treatments NO, AR and BW operate via the first and/or second mechanisms. The anomalous behavior of the BW group with respect to the quenchants cannot be explained without further investigation. The DI surface treatment apparently covers the surface with a large density of chemisorbed oxygen and causes a strong inversion region.

It is now assumed, along with Jäntsch,[32] that after the etching, quenching and surface treatment, the silicon surface is covered with a large density of chemisorbed water molecules and a much smaller density of oxygen molecules. Then, prior to any significant exposure to air, the energy bands will be bent slightly downwards at the surface.

During the evacuation for the gold electrode evaporation, the chemisorbed impurities are partially desorbed. Gibbons[20] has indicated that the energy of the gold atoms impinging on the surface during gold deposition may be sufficient to dislodge chemisorbed atoms or molecules so that the desorption may be greater under the gold electrode than at the free surface. During exposure

to air after gold deposition, oxygen and water are chemisorbed again. However, now the adsorption characteristics are different under the gold electrode than at the free surface. It is here that the metal work function enters the picture. The electric field due to the difference in work functions of the gold and silicon will be such as to attract negative ions towards the silicon surface and to repel positive ions away from it. Thus, one or both of the following two effects will take place. If the water molecules or oxygen atoms are ionized while diffusing through the gold layer, then the electric field will help the diffusion of oxygen and retard that of water. Secondly, even if water and oxygen diffuse as neutral molecules and atoms respectively (it is known that diffusion of diatomic gases such as O_2, N_2 etc. takes place as atoms, not as molecules),[34] the electric field will aid the bonding or fixation of oxygen but will hinder that of water. Diffusion through the gold electrode must be assumed in order to explain the variation of the aging time with the thickness of the gold layer.[17] The above discussion then accounts for the aging time of only a few days for the high work function metals Au, Cr, Pt compared to several months for other low work function metals.

Usually, the exposure to vacuum during gold deposition is not more than 2-3 hours, and the vacuum is not very high (pressure $\sim 10^{-5}$-10^{-6} torr) so that there may not be a significant desorption of impurities and if the pre-gold-deposition exposure to air was negligible, then the bands may still be bending downwards at the

silicon surface soon after gold deposition, even under the gold electrode. The surface barrier will naturally exhibit a large reverse current under these conditions, as observed by Siffert and Coche.[15] During post-gold-deposition exposure to air, oxygen will preferentially diffuse through the gold electrode as discussed above. At the free surface, oxygen will gradually tend to displace much of the water over a period of several days. Maxwell and Green[33] have shown that such a displacement of water by oxygen takes place on germanium surfaces and it is therefore reasonable to assume that it also occurs on silicon surfaces. The rate of displacement depends on the surface treatment. On surfaces treated by the DI treatment, the oxygen displaces water rather rapidly whereas for the AR surface treatment, the displacement is the slowest. It is this period of oxygen diffusion through the gold and displacement at the free surface which comprises the aging period for a surface barrier.

During the aging process, the energy bands continue to bend upwards both at the free surface and under the gold electrode until some equilibrium values of V_s and V_d in air are reached. For surface barriers yielding low reverse currents, such as NOH, ARH etc., the condition $|V_d| > |V_s|$ is satisfied, with the proper value of $|V_d| - |V_s|$ to yield a high breakdown voltage for the reverse biased B_{sc}- F_{sc} junction. The condition $|V_d| > |V_s|$ is fulfilled because of the larger density of water molecules at the free surface than under the gold electrode. This also explains why

a certain amount of moisture in the air is necessary in order to yield low reverse current surface barriers. It also explains why the surface barrier which gives a low reverse current in air deteriorates considerably under a poor vacuum after only a short time of evacuation. Presumably, the bond-strength of the water molecules at the free surface is reduced after the displacement or aging process so that even a slight evacuation removes the water molecules, and increases $|V_s| \cdot |V_d|$ will remain essentially constant under a slight evacuation so that $|V_s|$ will approach $|V_d|$ and give rise to a large reverse current. The relative stability under a second exposure to vacuum after recovery in air can be explained by the fact that recovery takes place due to the displacement of some of the oxygen by water which now has a tighter bonding than before. Jäntsch[32] observed that water molecules can permeate chemisorbed oxygen and reach the silicon surface. The exact mechanism of displacement of water by oxygen or of oxygen by water and of the ensuing bond strengths is not well understood.

Finally, the deterioration of surface barriers under electropositive vapors such as NH_3 and HF can be explained on the basis of the B_{sc}- F_{sc} junction breaking down at very low voltages. This is due to a large density of electrons in the free surface space charge region and a high density of holes in the barrier space charge region. The surface channel current is significantly controlled by the B_{sc}- F_{sc} breakdown voltage even at voltage values well below this breakdown voltage because of the avalanche

multiplication in the reverse biased B_{sc}- F_{sc} junction. The lowest surface channel current is obtained when F_{sc} is highly depleted and B_{sc} is slightly inverted. When this happens, the total reverse current is then given mainly by the bulk diffusion and depletion region generation currents of the surface barrier proper, as shown by Langmann and Mayer.[26]

Conclusions

The following conclusions can be drawn with reference to the previously stated motivations behind the work reported here.

I. The experimental results allow us to make a comparative evaluation of the different fabrication techniques for surface barriers. We then find that:

1) The NO surface treatment is superior to the other treatments tested. It can also be said that regardless of the type of surface treatment used, a few days of storage in high resistivity deionized water yields superior diodes than does a pre-gold-deposition exposure to air.

2) For the NO and AR surface treatments, the HF quenchant is superior to the normally used H_2O quenching procedure.

3) Any exposure to air prior to the gold electrode deposition is unnecessary.

II. With reference to the previously stated unresolved problems regarding the effects of surface treatments, quenchants, ambients, and metal work functions on the rectification

characteristics of surface barrier diodes, the following statements can be made.

1) The model presented above accounts quite well for the necessity of exposure to both air and moisture (that is, to normal humid air, not dry air) in order to yield low reverse currents. Regarding the amount and sequence of exposure, an exposure of a few days after gold deposition is sufficient. Effects of other gases and vapors can also be explained on the basis of their relative influences on V_s and V_d. Ambient insensitivity can be achieved only by proper encapsulation.

2) The mechanism by which the chemical surface treatments operate is mainly by controlling the sticking coefficients of different ambients although it is also possible that the surface treatment has some influence on the energy positions of the fast states.

3) The role of the metal work function is believed to be that of causing preferential adsorption of certain ambients, so as to maintain the equilibrium value of $|V_d|$ larger than that of $|V_s|$. On the whole, the metal work function is of secondary importance compared to the surface treatment, quenchant and ambients.

4) The reverse current does not depend directly on the barrier height; rather, it depends on the relative magnitudes of $|V_d|$ and $|V_s|$. Even the true surface barrier current, aside from the surface channel current, does not depend exponentially on the diffusion potential V_d as predicted by the Schottky theory.

Thus, there is a strong experimental evidence that the surface barrier behaves like a regular p-n junction diode.

(5) Archer's results regarding increasing film thickness in going from an HNO_3 quenched surface to an H_2O quenched surface seem to be confirmed. It also appears that HF quenching gives a still thicker film, at least for the NO, AR and DI surface treatments. The mechanism by which the quenchants control the rectification characteristics is by controlling the surface density of fast surface states.

III. The simple model presented above does explain most of the observed effects. These have already been discussed.

Recommendations for Further Research

Further work can be performed on the Au-n-Si in the following areas.

1. Theoretical work can be done in order to obtain quantitative relationships between V_s, V_d, and the reverse current and breakdown voltage. V_s, V_d should in turn, be possible to obtain from the densities of slow states and the densities and energy positions of fast states. Obtaining the value of V_d will also require a knowledge of the thicknesses and dielectric constants of the interfacial layers.

2. More work should be performed on the chemical aspects of the behavior of surface treatments, quenchants and ambients.

3. An attempt should be made of performing the same type

of measurements as reported here except that the surface barrier and field effect sample should both be parts of the same filament, as shown in Fig. 21. Then, field effect and current voltage measurements can be simultaneously performed under any given ambient.

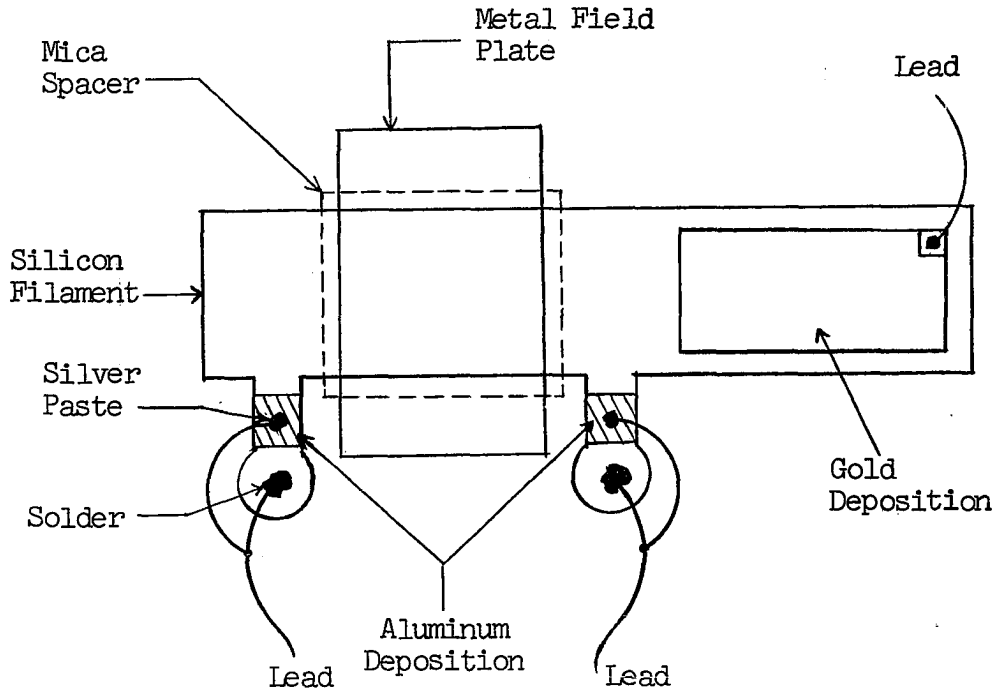

Figure 21

The contacts for the FE measurements should be made to the bulk as well as to the surface so as to eliminate the inaccuracy of FE measurements. The surface contact is made with silver paste on evaporated aluminum whereas the bulk contact should be made by soldering on a roughened-up surface.

REFERENCES

1. J. W. Mayer and B. R. Gossick, Rev. Sci. Instr., 27 467 (1956) J. W. Mayer, J. Appl. Phys., 30, 1937 (1959).

2. K. G. McKay, Phys. Rev., 84, 829 (1951).

3. E. D. Klema, Nuclr. Instr. & Methods, 26, 205 (1964).

4. C. P. Goradia and J. Reynolds, Paper presented at the Eleventh Scintillation and Semiconductor Counter Symposium, Washington D.C., Feb. 1968, to be published in IEEE Trans. Nuc. Sci., June, 1968.

5. G. Dearnaley and D. C. Northrop, "Semiconductor Counters for Nuclear Radiations," second edition, Barnes and Noble Inc., New York.

6. F. S. Goulding, Nuclr. Instr. & Methods, 43, 1 (1966).

7. J. W. Mayer, Nuclr. Instr. & Methods, 43, 55 (1966).

8. W. L. Brown et al in "Semiconductor Surface Physics," R. H. Kingston ed., University of Pennsylvania Press, Philadelphia (1956).

9. H. K. Henisch, "Rectifying Semiconductor Contacts," Oxford University Press, 205 (1957).

10. E. Spenke, "Electronic Semiconductors," McGraw-Hill Book Co., New York, 102 (1958).

11. J. Bardeen, Phys. Rev., 71, 717 (1947).

12. I. Tamm, Physik. Zeits. Sowjetunion, 1, 733 (1932).

13. W. Shockley, Phys. Rev., 56, 324 (1939).

14. C. A. Mead and W. G. Spitzer, Phys. Rev., 134, A713 (1964).

15. P. Siffert and A. Coche, IEEE Trans. Nucl. Sci., NS-12, 284 (1965).

16. A. Many, Y. Goldstein and N. B. Grover, "Semiconductor Surfaces," North Holland Publishing Co., Amsterdam (1965).

17. P. Siffert and A. Coche, IEEE Trans. Nucl. Sci., NS-11, 244 (1964).

18. J. Reynolds and B. Persson, Nucl. Instr. & Methods, 33, 77 (1965).

19. F. J. Walter and R. R. Boshart, IEEE Trans. Nucl. Sci., NS-13, 189 (1966).

20. P. E. Gibbons, Nucl. Instr. & Methods, 29, 289 (1964).

21. R. J. Archer, J. Phys. Chem. Solids, 14, 104 (1960).

22. A. M. Cowley and S. M. Sze, J. Appl. Phys., 36, 3212 (1965).

23. F. J. Walter and R. R. Boshart, Nucl. Instr. & Methods, 42, 1 (1966).

24. J. Lindmayer and C. Y. Wrigley, "Fundamentals of Semiconductor Devices," D. Van Nostrand Publishing Co., Princeton, N. J. (1965).

25. C. T. Sah, R. N. Noyce and W. Shockley, Proc. IRE, 45, 1228 (1957).

26. H. J. Langmann and O. Meyer, Nucl. Instr. & Methods, 44, 55 (1966).

27. R. H. Kingston and S. F. Neustadter, J. Appl. Phys., 26, 718 (1955).

28. J. R. Schrieffer, Phys. Rev., 97, 641 (1955).

29. C. A. Klein, paper presented at the Eleventh Scintillation and Semiconductor Counter Symposium, Washington D.C., Feb. 1968, to be published in IEEE Trans. Nucl. Sci., NS-15, June, 1968.

30. J. Blakemore, "Semiconductor Statistics," Pergamon Press, New York (1962).

31. W. L. Brown, Phys. Rev., 100, 590 (1955).

32. O. Jäntsch, J. Phys. Chem. Solids, 26, 1233 (1965).

33. K. H. Maxwell and M. Green, J. Phys. Chem. Solids, 14, 94 (1960).

34. W. Jost, "Diffusion in Solids, liquids, gases," Academic Press, New York, 1960.